A Universal Design of Betacoronavirus Vaccines against COVID-19, MERS, and SARS

Graphical Abstract
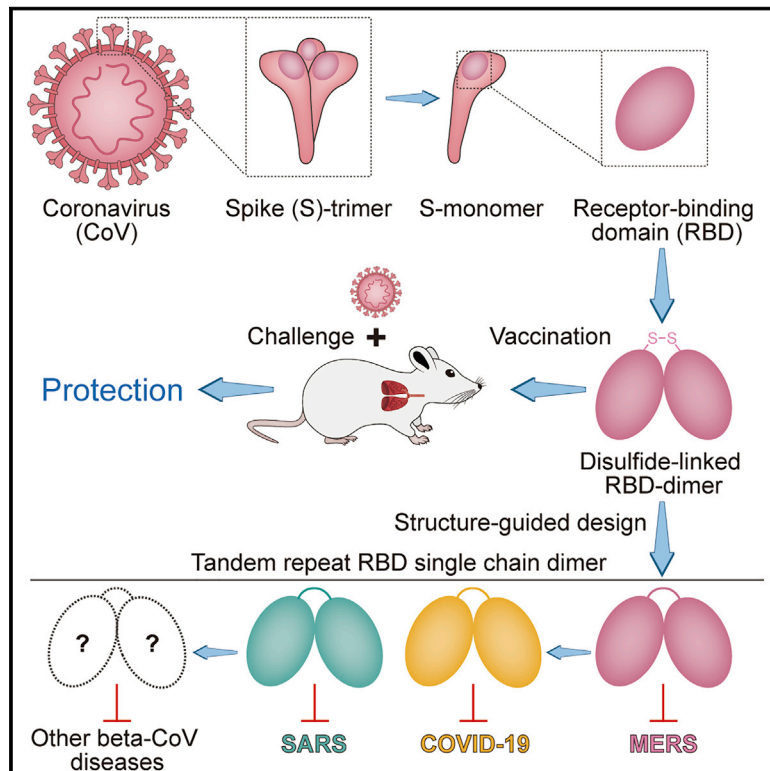
Authors
Lianpan Dai, Tianyi Zheng, Kun Xu, ..., Chuan Qin, Jinghua Yan, George F. Gao

Correspondence
dailp@biols.ac.cn (L.D.),
qinchuan@pumc.edu.cn (C.Q.),
yanjh@im.ac.cn (J.Y.),
gaof@im.ac.cn (G.F.G.)

In Brief
Gao et al. present the structure-guided design of a coronavirus immunogen comprised of two protein subunits each containing the virus spike receptor binding domain fused together via a disulfide link or tandem repeat. The immunogen elicits strong immunogenicity in mice and protects them against viral challenge. The vaccine design strategy can be universally applied to SARS, MERS, COVID-19, and other CoV vaccines to counter emerging threats.

Highlights

- A dimeric form of MERS-CoV RBD is highly immunogenic and protective in mice

- RBD-dimer structure guides further design of a homogeneous dimer by tandem repeat

- The strategy is generalizable to design beta-CoV vaccines against COVID-19 and SARS

- CoV RBD-dimer immunogens can be produced at high yields in pilot scale production

CellPress

Article

A Universal Design of Betacoronavirus Vaccines against COVID-19, MERS, and SARS

Lianpan Dai,[1,2,3,12,*] Tianyi Zheng,[1,2,12] Kun Xu,[3,12] Yuxuan Han,[2,12] Lili Xu,[4,12] Enqi Huang,[5] Yaling An,[1] Yingjie Cheng,[5] Shihua Li,[6] Mei Liu,[7] Mi Yang,[7] Yan Li,[6] Huijun Cheng,[1] Yuan Yuan,[6] Wei Zhang,[6] Changwen Ke,[8] Gary Wong,[9,10] Jianxun Qi,[2,6] Chuan Qin,[4,*] Jinghua Yan,[6,7,*] and George F. Gao[1,2,6,11,13,*]

[1]Research Network of Immunity and Health (RNIH), Beijing Institutes of Life Science, Chinese Academy of Sciences, Beijing 100101, China
[2]Savaid Medical School, University of Chinese Academy of Sciences, Beijing 101408, China
[3]Key Laboratory of Tropical Translational Medicine of Ministry of Education, School of Tropical Medicine and Laboratory Medicine, The First Affiliated Hospital, Hainan Medical University, Hainan 571199, China
[4]Key Laboratory for Animal Models of Emerging and Remerging Infectious Diseases, Institute of Laboratory Animal Science, Chinese Academy of Medical Sciences and Comparative Medicine Center, Peking Union Medical College, Beijing 100032, China
[5]Anhui Zhifei Longcom Biopharmaceutical Co. Ltd, Anhui 230088, China
[6]CAS Key Laboratory of Pathogenic Microbiology and Immunology, Institute of Microbiology, Chinese Academy of Sciences, Beijing 100101, China
[7]CAS Key Laboratory of Microbial Physiological and Metabolic Engineering, Institute of Microbiology, Chinese Academy of Sciences, Beijing 100101, China
[8]Guangdong Provincial Center for Disease Control and Prevention, Guangzhou 511430, China
[9]Institut Pasteur of Shanghai, Chinese Academy of Sciences, Shanghai 200031, China
[10]Department of Microbiology-Infectiology and Immunology, Laval University, Quebec City, QC G1V 4G2, Canada
[11]Chinese Center for Disease Control and Prevention (China CDC), Beijing 102206, China
[12]These authors contributed equally
[13]Lead Contact
*Correspondence: dailp@biols.ac.cn (L.D.), qinchuan@pumc.edu.cn (C.Q.), yanjh@im.ac.cn (J.Y.), gaof@im.ac.cn (G.F.G.)
https://doi.org/10.1016/j.cell.2020.06.035

SUMMARY

Vaccines are urgently needed to control the ongoing pandemic COVID-19 and previously emerging MERS/SARS caused by coronavirus (CoV) infections. The CoV spike receptor-binding domain (RBD) is an attractive vaccine target but is undermined by limited immunogenicity. We describe a dimeric form of MERS-CoV RBD that overcomes this limitation. The RBD-dimer significantly increased neutralizing antibody (NAb) titers compared to conventional monomeric form and protected mice against MERS-CoV infection. Crystal structure showed RBD-dimer fully exposed dual receptor-binding motifs, the major target for NAbs. Structure-guided design further yielded a stable version of RBD-dimer as a tandem repeat single-chain (RBD-sc-dimer) which retained the vaccine potency. We generalized this strategy to design vaccines against COVID-19 and SARS, achieving 10- to 100-fold enhancement of NAb titers. RBD-sc-dimers in pilot scale production yielded high yields, supporting their scalability for further clinical development. The framework of immunogen design can be universally applied to other beta-CoV vaccines to counter emerging threats.

INTRODUCTION

In recent years, we have faced unprecedented threats by coronavirus (CoV) infections. During 2002–2004, severe acute respiratory syndrome CoV (SARS-CoV) was first reported in China and resulted in more than 8,000 infections worldwide with ~800 related deaths (https://www.who.int/). In 2012, Middle East respiratory syndrome CoV (MERS-CoV) emerged from Saudi Arabia and quickly spread into 27 countries, with an even higher fatality rate of 34.4%. Infections of humans by MERS-CoV were still being reported recently (https://www.who.int/csr/don/archive/disease/coronavirus_infections/en/). Currently, coronavirus disease in 2019 (COVID-19) caused by SARS-CoV-2 infection is classified as a pandemic, spreading to 216 countries with 6,140,934 laboratory-confirmed cases and 373,548 deaths (as of June 2, 2020, from https://www.who.int/) (Wang et al., 2020a; Wei et al., 2020; Zhu et al., 2020). The outbreak is still growing rapidly. In addition, more and more SARS- and MERS-related CoVs were identified in animal reservoir raising the concerns for their zoonotic transmissions and pandemic potential in future (Banerjee et al., 2019; Wong et al., 2019).

CoVs are a diverse group of enveloped viruses, which are further subdivided into four genera, alpha-, beta-, gamma-, and delta-CoV (Knipe and Howley, 2013; Woo et al., 2009) (https://talk.ictvonline.org/). To date, seven CoVs are known to cause human diseases (Lu et al., 2015; Wevers and van der Hoek, 2009). Among them, two alpha-CoVs (hCoV-NL63 and
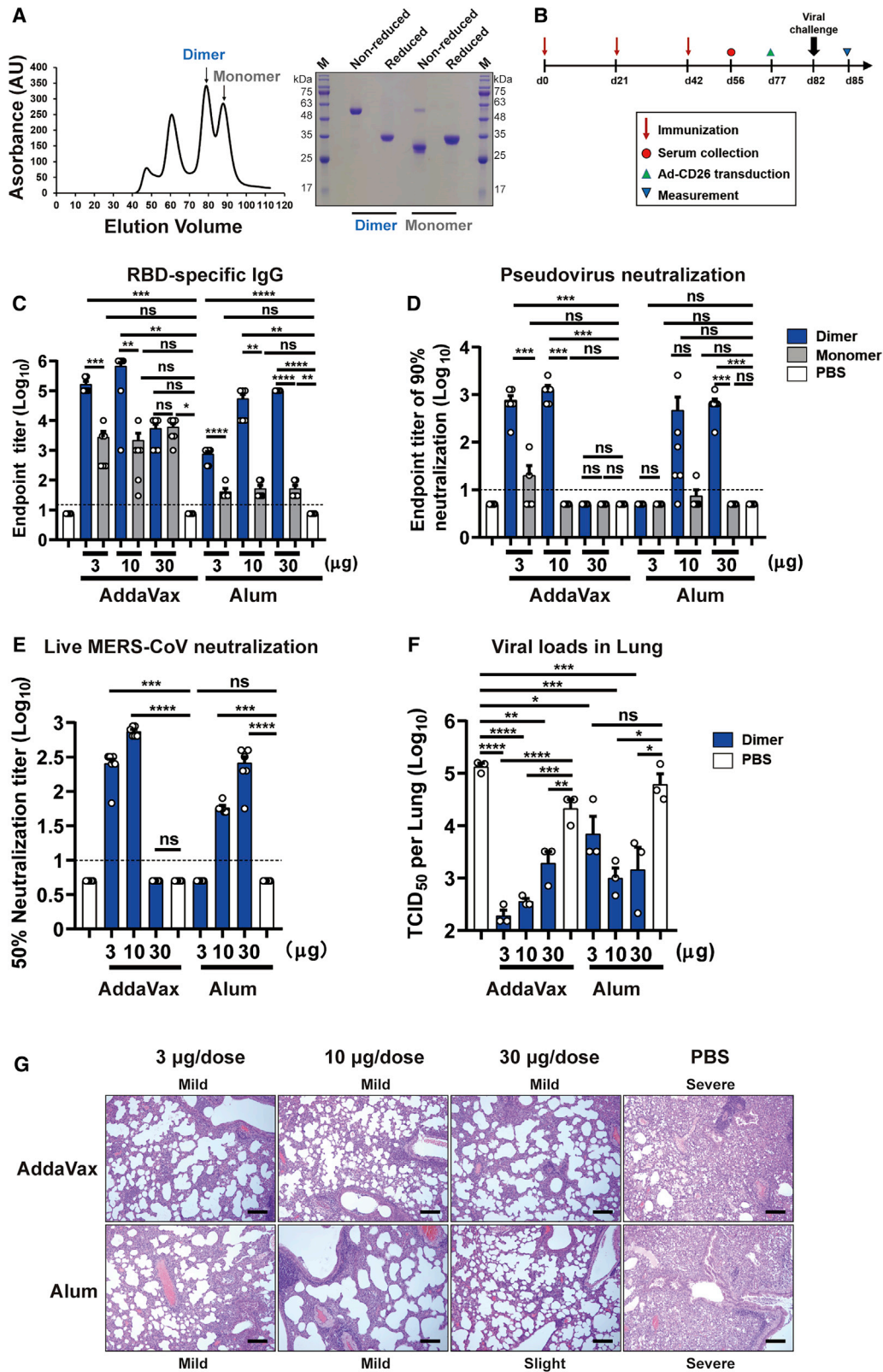
(legend on next page)

hCoV-229E) and two beta-CoVs (HCoV-OC43 and HKU1) only cause self-limiting cold-like illnesses (Chiu et al., 2005; Gorse et al., 2009; Jean et al., 2013; Jevšnik et al., 2012). However, the remaining three beta-CoVs (SARS-CoV, MERS-CoV, and SARS-CoV-2) are life-threatening. To date, no clinically effective prophylactics or therapeutics are available for the prevention or treatment of the highly pathogenic CoV infections in human, highlighting the urgent need for vaccine development.

In CoVs, the envelope-embedded spike (S) proteins are responsible for recognition of host cellular receptors to initiate virus entry (Lu et al., 2015). The receptor-binding domain (RBD) of S protein is required for the receptor docking. SARS-CoV and SARS-CoV-2 use the same functional host cellular receptor, human angiotensin converting enzyme 2 (hACE2) (Hoffmann et al., 2020; Li et al., 2003; Walls et al., 2020; Wang et al., 2020c), whereas, MERS-CoV uses human CD26 (also known as human dipeptidyl peptidase 4, hDPP4) (Lu et al., 2013; Raj et al., 2013). We and others have previously revealed the structural bases for the receptor-recognition by these CoVs (Lan et al., 2020; Li et al., 2005a; Lu et al., 2013; Shang et al., 2020; Wang et al., 2013, 2020c; Yan et al., 2020). So far, most of potent neutralizing monoclonal antibodies are against CoV RBD (Jiang et al., 2020; Li et al., 2015; Modjarrad et al., 2016). Therefore, RBD is an attractive vaccine target because it can focus the immune response on interference of receptor binding (Jiang et al., 2012; Wang et al., 2020b; Zhang et al., 2015; Zhou et al., 2019b). To date, a number of RBD-based vaccines have been reported in development against MERS and SARS (Jiang et al., 2012; Wang et al., 2020b; Zhou et al., 2019b). However, RBD-based subunit vaccines may face some important challenges, mostly arising from their relatively low immunogenicity, which must be combined with appropriate adjuvants or optimized for suitable protein sequences, fragment lengths, and immunization schedules (Wang et al., 2020b). Strategies to promote immunogenicity of RBD-based vaccine include increasing the antigen size, multimerization or intensive antigen-display in particles, however, these strategies inevitably introduced exogenous sequences which complicated their potentials for clinical usage (Du et al., 2007, 2013; He et al., 2004; Kim et al., 2018; Li et al., 2019; Ma et al., 2014; Nyon et al., 2018; Tai et al., 2016; Tang et al., 2015; Wang et al., 2017).

Here, we describe a universal design of beta-CoV immunogens that overcomes the immunogenicity limitation of RBD-based vaccine. CoV RBD dimers have been observed before (Hwang et al., 2006; Lan et al., 2020; Xiao et al., 2004; Zhang et al., 2018), but their immunogenicity has not been tested. We found a disulfide-linked dimeric form of MERS-CoV RBD significantly enhanced the antibody response and neutralizing antibody (NAb) titer compared to the conventional monomeric form. In a mouse model, it conferred protection against MERS-CoV infection and relieved lung injury. Crystal structure revealed the RBD-dimer fully exposed dual receptor binding motifs (RBMs), the major site recognized by NAbs. To increase dimer stability, the immunogen was further engineered as a version of tandem repeat single chain dimer (sc-dimer) by structure-guided design without introducing any exogenous sequence. The RBD-sc-dimer retained high vaccine efficacy as the disulfide-linked dimer. Next, this strategy was further generalized to develop vaccines against the other two highly pathogenic beta-CoVs, SARS-CoV-2 and SARS-CoV. Notably, RBD-sc-dimer design significantly increased the immunogenicity and enhanced NAb titers between 10- to 100-fold compared to the conventional RBD-monomer, indicating its feasibility as a universal strategy for beta-CoV vaccine design. In particular, two doses of RBD-sc-dimer elicited high NAb titers up to ~4,096 against SARS-CoV-2 infection. The RBD-sc-dimers of MERS-CoV and SARS-CoV-2 were further developed for pilot scale production in GMP grade manufacturing. Both can be produced at high yields (g/L level) in an industry-standard Chinese hamster ovary (CHO) cell system, suggesting its scalability and promise for further clinical development to control MERS and the ongoing COVID-19 pandemic.

RESULTS

Identification of a Dimeric Form of MERS-CoV RBD as a Superior Immunogen

Our initial aim was to develop an RBD-based MERS vaccine. MERS-CoV RBD (E367-Y606) was expressed by baculovirus in insect cells. The supernatant was harvested and the secreted proteins were purified. Analytical gel filtration indicated a supposed RBD monomer-dimer equilibrium in solution, and their protein sizes were further confirmed by gel electrophoresis as ~30 kDa and ~60 kDa, respectively (Figure 1A). An inter-molecule disulfide bond was required for the dimer formation as verified by

Figure 1. Dimeric Form of MERS-CoV RBD Enhances Immunogenicity and Is Protective in Mice

(A) Left: analytical gel filtration profile of baculo-derived MERS-CoV RBD (E367-Y606) protein with HiLoad 16/600 Superdex 200 pg. The 280-nm absorbance curves are shown. The proposed peaks of RBD-dimer and RBD-monomer are indicated with arrows. Right: SDS-PAGE migration profiles of RBD-dimer and -monomer proteins at non-reduced and reduced conditions.

(B) Time course of MERS vaccine immunization, viral challenge and measurement. Groups of 6- to 8-week-old female BALB/c mice (n = 6) were vaccinated with three doses of 3, 10, or 30 µg immunogen with adjuvant of AddaVax or Alum in 3-week intervals. PBS with and without adjuvant were given as controls. Serum samples were collected 14 days after last immunization. Mice were then transduced with 2.5×10^8 PFU of Ad5-hCD26 via i.n. route followed by infection with 5×10^5 PFU of MERS-CoV via i.n. route. Lung tissues were harvested and split for virus titer detection (n = 3) and pathological examination (n = 3), respectively.

(C) Enzyme-linked immunosorbent assay (ELISA) assay shows the RBD specific IgG titers.

(D) MERS-CoV pseudovirus neutralization assay shows the NT_{90}.

(E) MERS-CoV (EMC2012 strain) neutralization assay shows the NT_{50}.

(F) Virus titers in lung.

(G) Histology of lung sections (100-fold magnification). The lung injuries are marked as slight, mild, and severe, according to the degree of interstitial pneumonia. Black bar represents 100 µm.

The values shown in (C)–(F) are the mean ± SEM. The horizontal dashed line indicates the limit of detection. P-values were analyzed with one-way ANOVA (ns, $p > 0.05$; *$p < 0.05$; **$p < 0.01$; ***$p < 0.001$; ****$p < 0.0001$).
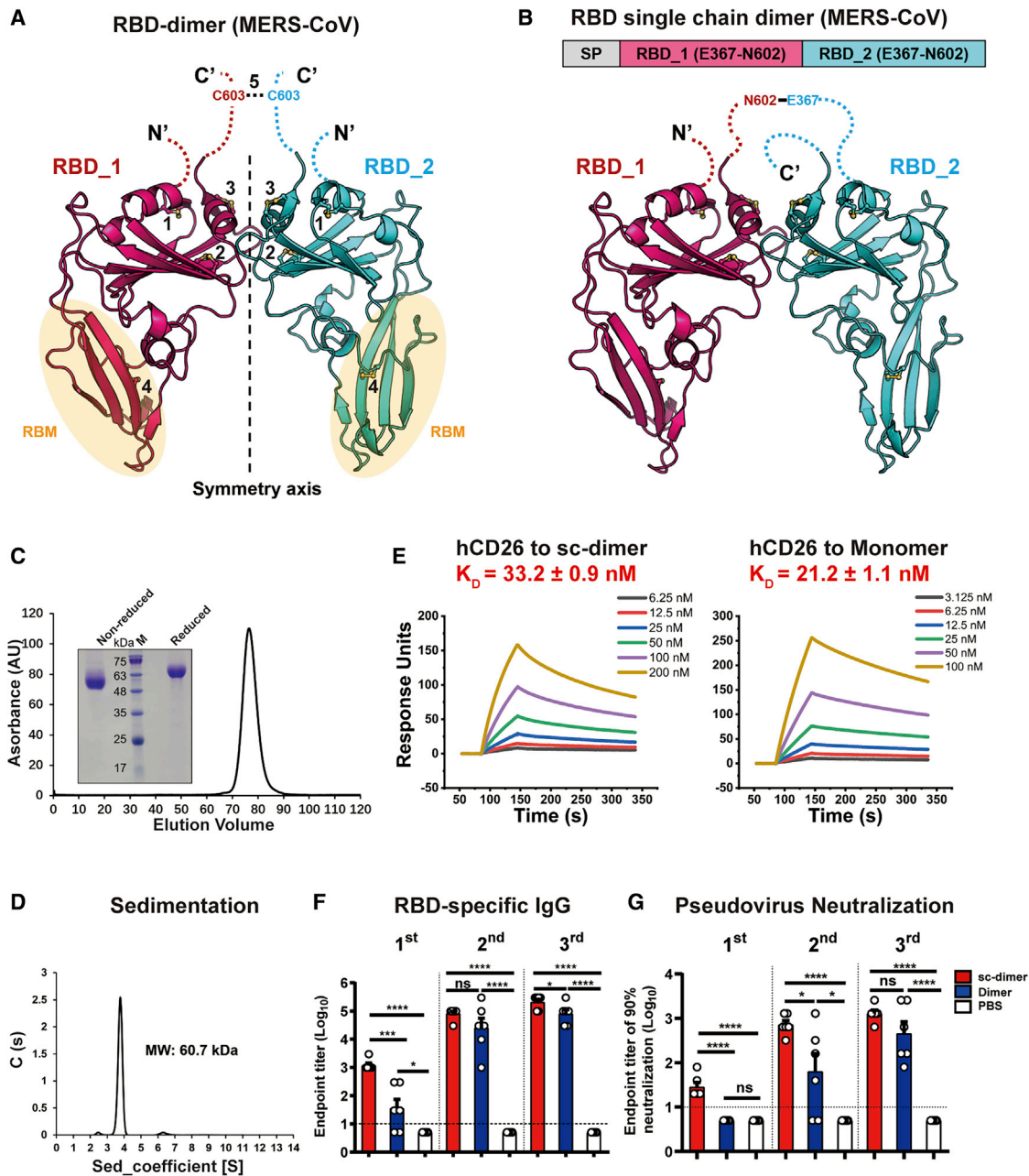
Figure 2. Structural Characterization of MERS-CoV RBD-Dimer and Structure-Guided Design of RBD-SC-Dimer as a MERS Vaccine

(A) A cartoon representation of the MERS-CoV RBD-dimer structure. Two RBD protomers are arranged in axial symmetry and are colored in hot pink and cyan, respectively. Intra- and inter-molecular disulfide bonds are numbered. Dashed loops represent the N- and C-terminal residues that are invisible in the electron density maps. The cysteine residue C603 is highlighted. The light yellow ellipses represent the regions of RBM.

(B) The schematic representation of MERS-CoV RBD-sc-dimer. RBDs are truncated at C-terminal residue N602 and connected as tandem repeat to form a single chain dimer (SP, signal peptide).

(C) Analytical gel filtration profile of MERS-CoV RBD-sc-dimer protein with HiLoad 16/600 Superdex 200 pg. The 280-nm absorbance curve is shown. Non-reduced and reduced SDS-PAGE migration profiles of the pooled samples are shown.

(D) Ultracentrifugation sedimentation profiles of MERS-CoV RBD-sc-dimer.

(E) Representative BIAcore diagrams of MERS-CoV RBD-sc-dimer and RBD-monomer bound to hCD26 protein. The K_D value was calculated by the software BIAevaluation Version 4.1 (GE Healthcare). The values shown are mean ± SD of two independent experiments.

(F and G) Groups of 6- to 8-week-old female BALB/c mice (n = 6) were immunized with a 10-μg dose of RBD-sc-dimer and HEK293T-derived disulfide-linked RBD-dimer, respectively, with AddaVax as adjuvant. PBS formulated with adjuvant was given as control. A three-dose vaccination regimen was performed. Serum samples were collected after each immunization (19 days after 1st immunization, 14 days after 2nd immunization, and 14 days after 3rd immunization) to

(legend continued on next page)

the dimer-to-monomer switch from non-reduced to reduced condition in gel electrophoresis (Figure 1A). To evaluate their potential as vaccines, increasing doses of RBD-dimer or -monomer were given to BALB/c mice, with the combination of AddaVax (an MF-59-like squalene adjuvant) or Alum as adjuvant. PBS plus adjuvant and PBS alone were given as controls. Serum samples were collected 14 days after the last immunization as indicated (Figure 1B). As expected, RBD-monomer is poorly immunogenic and induced low levels of antigen-specific antibody and NAb titer against pseudotyped virus (Figures 1C and 1D). In contrast, the dimer immunogen markedly enhanced the immunogenicity for both antibody responses and neutralization, with the 90% neutralization titer (NT_{90}) up to ~1,000 (Figures 1C and 1D). Because RBD-dimer was superior to monomer as an immunogen, sera from the dimer group were further tested for the neutralizing activities against live MERS-CoV virus (EMC2012 strain). Consistently, high levels of NAbs were detected in RBD-dimer-vaccinated mice using either AddaVax or Alum as adjuvant (Figure 1E). In particular, AddaVax combined with 10 μg dose of antigen reached NAb titers up to ~900 (Figure 1E).

Validation of Vaccine Protection for MERS-CoV RBD-Dimer *In Vivo*

To further explore the protective efficacy of RBD-dimer *in vivo*, the immunized mice were transduced via the intranasal (i.n.) route with adenovirus expressing hCD26 as the MERS-CoV-sensitive animal model (Figure 1B) (Zhao et al., 2014). Five days later, the transduced mice were intranasally challenged with 5×10^5 plaque-forming unit (PFU) of MERS-CoV. At 3 days after challenge, lung tissues were harvested for virus titer detection and pathological examination. Consistent with the high serological NAb titers in RBD-dimer-vaccinated mice, virus loads were reduced ~100- to 1,000-fold in lung compared to the PBS group (Figure 1F).

To further elucidate the protective effect of the vaccination, histopathological analyses were conducted on mice challenged with MERS-CoV. All lung tissue samples harvested from mice vaccinated with PBS exhibited severe interstitial pneumonia, pulmonary alveolitis, diffuse inflammatory cell infiltration, and necrosis of bronchial epithelial cells (Figure 1G). Milder lesions were observed in mice immunized with the RBD-dimer, because the pulmonary alveolus was highly visible with lower infiltration of inflammatory cells (Figure 1G). Therefore, RBD-dimer can substantially reduce the lung injury caused by MERS-CoV infection. The small histopathological changes in the lung likely resulted from a direct inoculation of high amount (5×10^5 PFU) of virus intranasally. Taken together, we demonstrated the RBD-dimer is a protective immunogen against MERS-CoV infection and has a significant improved immunogenicity.

Structural Characterization of MERS-CoV RBD-Dimer

To determine the molecular basis of the observed dimer immunogen at an atomic level, we determined the crystal structure of MERS-CoV RBD-dimer at a resolution of 2.9 Å (Table S1). Interestingly, RBD-dimer is arranged as a "bilateral-lung"-like structure with axial symmetry (Figure 2A). The dual RBMs are located at the lower lobes of both "lungs" facing outward against the axis (Figure 2A). Both RBMs are fully exposed (Figures 2A and S1), suggesting the potential to elicit antibodies interfering with receptor binding. The core subdomains of both RBD protomers stack on each other via α3 helices and loops surrounding the helices. The N and C termini are invisible in the electron density maps, indicating the flexibility of these regions. Accordingly, in the previously determined structure of the full-length MERS-CoV-S, these regions consist of flexible loops that facilitate the hinge-like conformational movements of RBD for receptor engagement (Yuan et al., 2017). Each RBD contains 9 cysteine residues, with 8 of them forming 4 intra-molecule disulfide bonds. An additional invisible C-terminal cysteine residue (C603) is proposed to build the inter-molecule disulfide bond covalently linking the RBD-dimer (Figure 2A). Given the number of flexible, unresolved residues that link the two subunits of the dimer together, and the small non-covalent interface observed between the two subunits of the dimer, it is far from certain that the crystallographically observed structure corresponds to a unique structure the protein adopts in solution.

Structure-Guided Design of the RBD-SC-Dimer

Because the RBD forms a monomer-dimer equilibrium in solution, the yields of dimer protein varied from batch to batch. To facilitate downstream vaccine development, we sought to further engineer the RBD-dimer in a more stable form. The structure of MERS-CoV RBD-dimer showed both N and C termini of two RBD protomers were juxtaposed and closed to each other (Figure 2A), which inspired us to link these two RBD as a tandem repeat single chain. In order to avoid introducing any exogenous sequences, we sought to link them by their own flexible terminal residues. Both RBDs were truncated at N602, the position just before C603 to avoid potential instability caused by cysteine residue, and then connected in tandem (Figure 2B). RBD expressed in a mammalian cell system was previously reported to be able to induce stronger neutralizing antibody response than those expressed in insect cells (Du et al., 2009b). We, therefore, constructed and expressed immunogens switching from insect cells to mammalian cells. The RBD-sc-dimer was expressed in mammalian HEK293T cells. The supernatant of the transfected cells was collected for further purification. Analytical gel filtration showed that the new construct was expressed as a single peak with a size of ~60 kDa, indicating the dimeric form of RBD (Figure 2C). The molecular weight was further corroborated as 60.7 kDa by analytical ultracentrifugation (Figure 2D). Surface plasmon resonance (SPR) assay demonstrated the RBM is exposed in the RBD-sc-dimer as in conventional RBD-monomer, supported by the comparable binding affinities of RBD to its receptor hCD26 (Figure 2E).

evaluate the humoral response dynamics. ELISA assay shows the MERS-CoV RBD-specific IgG titers in (F) and MERS-CoV pseudovirus neutralization assay shows the NT_{90} in (G). The values shown in (F) and (G) are the mean ± SEM. The horizontal dashed line indicates the limit of detection. P values were analyzed with one-way ANOVA (ns, $p > 0.05$; *$p < 0.05$; **$p < 0.01$; ***$p < 0.001$).
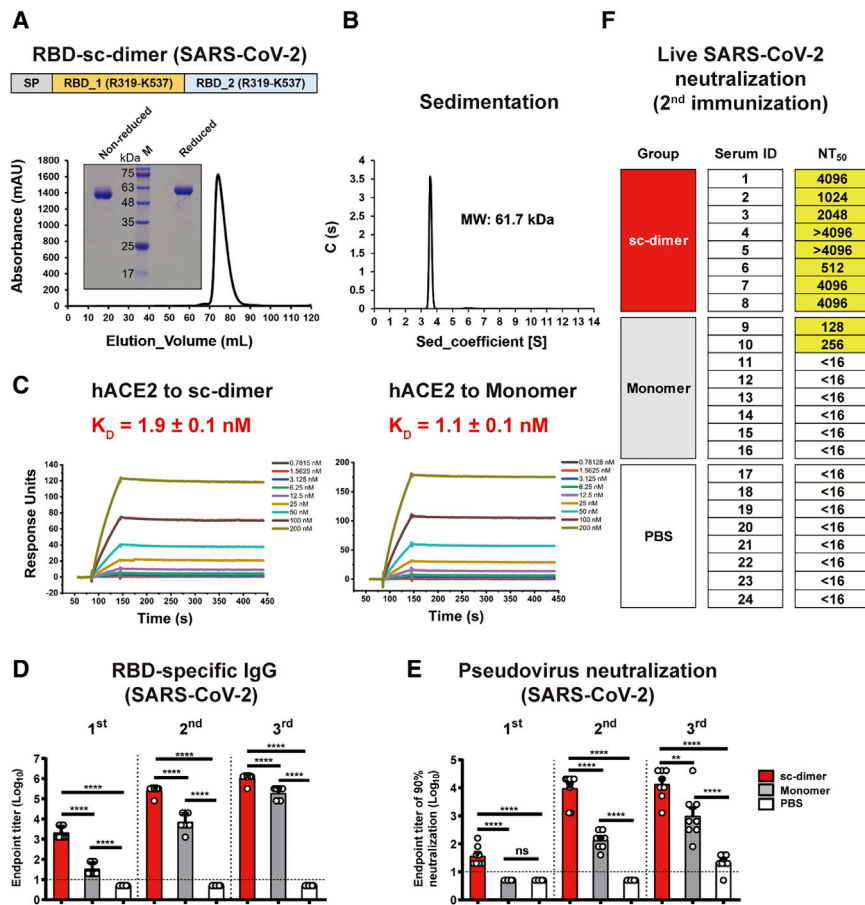See also Figure S1 and Table S1.

A
RBD-sc-dimer (SARS-CoV-2)

| SP | RBD_1 (R319-K537) | RBD_2 (R319-K537) |

B
Sedimentation

MW: 61.7 kDa

F
Live SARS-CoV-2 neutralization (2nd immunization)

Group	Serum ID	NT$_{50}$
sc-dimer	1	4096
	2	1024
	3	2048
	4	>4096
	5	>4096
	6	512
	7	4096
	8	4096
Monomer	9	128
	10	256
	11	<16
	12	<16
	13	<16
	14	<16
	15	<16
	16	<16
PBS	17	<16
	18	<16
	19	<16
	20	<16
	21	<16
	22	<16
	23	<16
	24	<16

C
hACE2 to sc-dimer
$K_D = 1.9 \pm 0.1$ nM

hACE2 to Monomer
$K_D = 1.1 \pm 0.1$ nM

D
RBD-specific IgG (SARS-CoV-2)
1st   2nd   3rd

E
Pseudovirus neutralization (SARS-CoV-2)
1st   2nd   3rd

■ sc-dimer
■ Monomer
□ PBS

Figure 3. Design and Assessment of RBD-SC-Dimer as a Vaccine against SARS-CoV-2

(A) A schematic diagram of SARS-CoV-2 RBD-sc-dimer. Two SARS-CoV-2 RBD (R319-K537) were dimerized as tandem repeat (SP, signal peptide). Analytical gel filtration of SARS-CoV-2 RBD-sc-dimer protein was performed with HiLoad 16/600 Superdex 200 pg. The 280-nm absorbance curve is shown. Non-reduced and reduced SDS-PAGE migration profiles of the pooled samples are shown.

(B) Ultracentrifugation sedimentation profiles of SARS-CoV-2 RBD-sc-dimer.

(C) Representative BIAcore diagrams of SARS-CoV-2 RBD-sc-dimer and monomer bound to hACE2 protein. The K_D value was calculated by the software BIAevaluation Version 4.1 (GE Healthcare). The values shown are mean ± SD of two independent experiments.

(D and E) Groups of BALB/c mice were immunized with a 10-μg dose of SARS-CoV-2 RBD-sc-dimer and conventional RBD-monomer, respectively, with AddaVax as adjuvant. PBS formulated with adjuvant was given as control. A three-dose vaccination regimen was performed. Serum samples were collected after each immunization (19 days after 1st immunization, 14 days after 2nd immunization, and 14 days after 3rd immunization) to evaluate the humoral response dynamics. ELISA assay shows the SARS-CoV-2 RBD specific IgG titers in (D) and SARS-CoV-2 pseudovirus neutralization assay shows the NT$_{90}$ in (E). The values shown in (D) and (E) are the mean ± SEM. The horizontal dashed line indicates the limit of detection. P-values were analyzed with one-way ANOVA (ns, $p > 0.05$; *$p < 0.05$; **$p < 0.01$; ***$p < 0.001$; ****$p < 0.0001$).

(F) Evaluation of neutralization activity with live SARS-CoV-2. The serum samples of RBD-sc-dimer, RBD-monomer, and control groups from the second immunization were serially diluted and mixed with 100 50% tissue culture infectious dose (TCID$_{50}$) SARS-CoV-2 (2020XN4276 strain). The mixtures were added into Vero cells and cytopathic effects (CPE) could be observed 72 h post infection. The NT$_{50}$ was calculated as reciprocal of serum dilution required for 50% neutralization of viral infection.
See also Figures S2 and S3.

To assess the immunogenicity of the RBD-sc-dimer, we immunized mice with 10 μg dose of antigen formulated with AddaVax as adjuvant. Equivalent HEK293T-derived disulfide-linked RBD-dimer was given as a comparison. PBS plus adjuvant was used as the control. We performed a three-dose regimen to assess the response dynamics. Impressively, the sc-dimer immunogen can elicit RBD-specific IgG up to endpoint titer of ~10^5 after the second and third immunizations, which was marginally higher than that induced by the original disulfide-linked RBD-dimer (Figure 2F). Serum samples were further tested for their neutralizing activities using pseudotyped virus. The RBD-sc-dimer induced NT$_{90}$ up to ~1,000 after both two and three injections, which were also marginally higher than that induced by the disulfide-linked RBD-dimer (Figure 2G). Two immunizations reached almost the peak antibody response for the sc-dimer-vaccinated mice (Figures 2F and 2G). Taken together, the RBD-sc-dimer was highly immunogenic and maintained the vaccine potency comparable to, if not slightly higher than, that of the original disulfide-linked RBD-dimer.

The RBD-SC-Dimer Strategy Applied to Vaccine Design against SARS-CoV-2 and SARS-CoV

Because the three life-threatening CoVs identified to date all belong to beta-CoV, we further explored the potential of RBD-sc-dimer strategy for vaccine design against other CoVs in these genera. RBD sequences from 19 identified beta-CoVs were aligned together and showed the conserved cysteine residue at C603 position of MERS-CoV S protein (Figure S2). Next, we sought to design immunogens of RBD-sc-dimer against the other two highly pathogenic CoVs, SARS-CoV-2 and SARS-CoV.

The RBD construct for SARS-CoV-2 started at R319 (the E367 position of MERS-CoV S protein) and was truncated at C-terminal residue K537, the amino acid just before C603 position of MERS-CoV S protein (Figures 3A and S2). Two copies of RBD were then dimerized in tandem as the strategy described for MERS-CoV RBD-sc-dimer (Figure 3A). SARS-CoV-2 RBD was expressed as a single dimer-sized protein, as verified by analytical gel filtration and gel electrophoresis (Figure 3A). Further

analytical ultracentrifugation determined its molecular weight as 61.7 kDa, suggesting a stable dimer formation (Figure 3B). The SPR assay demonstrated RBD-sc-dimer bound to receptor hACE2 with comparable affinity as its monomer counterpart, implying the exposure of the RBMs (Figure 3C; Table S2). Interestingly, the hACE2 protein expressed by baculovirus from insect cells showed weaker affinities to bind SARS-CoV-2 RBDs (two orders of magnitude lower) compared to mammalian-derived one, suggesting different glycosylation patterns of the hACE2 proteins may account for the distinct binding affinities (Table S2).

To further assess the immunogenicity, we first immunized BALB/c mice with the SARS-CoV-2 RBD-sc-dimer or conventional RBD-monomer (10 μg dose of immunogen plus AddaVax adjuvant). PBS formulated with adjuvant was given as control. Three-dose regimens were performed to assess the response dynamics. Serum samples were collected after each immunization and measured for the humoral responses. As expected, the RBD-sc-dimer of SARS-CoV-2 induced a significantly higher antigen-specific IgG compared to the conventional RBD-monomer after each immunization (p < 0.0001) (Figure 3D). Consistently, RBD-sc-dimer elicited ~10- to 100-fold higher titers of NAb compare to monomer in an assay with pseudotyped virus (Figure 3E). Two immunizations almost maximized the NAb titer induced by RBD-sc-dimer (Figure 3E), therefore, we further tested neutralizing activities after the second immunization against live SARS-CoV-2 (2020XN4276 strain) infection. Impressively, all serum samples from RBD-sc-dimer group showed high NAb titers, with the 50% neutralization titer (NT_{50}) of most samples reaching 4,096 and above (Figure 3F). In contrast, only 2 out of 8 serum samples from RBD-monomer-vaccinated mice reached NAb titers beyond 16, to a maximum of 256 (Figure 3F). To characterize the cellular immune responses, enzyme-linked immunospot (ELISPOT) and intracellular cytokine staining (ICS) assays were performed. We could not detect substantial induction of T cell responses in RBD-sc-dimer-vaccinated mice compared to the PBS-vaccinated ones after the last vaccination (Figure S3).

In order to design RBD-sc-dimer for SARS-CoV, the RBD construct was started at R306 (the E367 positon of MERS-CoV S protein) and truncated at Q523, one residue ahead of the C603 position in the MERS-CoV S protein (Figure S2). Two copies of RBD were further linked as tandem repeat. The stable dimer was detected in analytical gel filtration and gel electrophoresis (Figure 4A), with a molecular weight of 54.5 kDa as determined by analytical ultracentrifugation (Figure 4B). SARS-CoV receptor hACE2 was found to bind RBD-sc-dimer with affinity comparable to its binding to RBD-monomer, suggesting the exposure of RBMs (Figure 4C; Table S3). We also evaluated the immunogenicity for RBD-sc-dimer of SARS-CoV compared with its monomeric form using the same three-dose vaccination regimen. Consistent with what was found in assessment of MERS and COVID-19 vaccines, RBD-sc-dimer significantly enhanced the antigen-specific antibody responses and NAb titers compared to the conventional RBD-monomer. This enhancement was pronounced after the second immunization (Figures 4D and 4E).

High Yields of RBD-SC-Dimer in an Industry-Standard CHO Cell System

In view of the ongoing COVID-19 pandemic and frequent MERS outbreaks, we sought to further develop vaccines against these two CoVs for pilot scale production in GMP grade manufacturing. The RBD-sc-dimers of MERS-CoV and SARS-CoV-2 were constructed without purification tag and subsequently transformed to clinical-grade CHO cell lines. Stable CHO cell lines were screened for antigen expression. Cell lines with highest antigen abundance were selected for large scale production. Notably, both RBD-sc-dimers can be produced at high yields, to the level of gram per liter. The RBD-sc-dimer of MERS-CoV reached expression levels of >2 g/L, with a final yield of 1.05 g purified antigen per liter (Figure 5A). The RBD-sc-dimer of SARS-CoV-2 can reach expression levels of >1.5 g/L, with a final yield of 0.67 g purified antigen per liter (Figure 5A). Both antigens reached >98% purity as verified by gel electrophoresis analyses (Figures 5A and 5B). The highly scalable production of these two immunogens strongly suggested the feasibility to meet the vaccine demands worldwide.

DISCUSSION

In general, the current CoV vaccine candidates can be classified into two categories: (1) gene-based vaccines including DNA/messenger RNA vaccines, recombinant vaccine vectors, and live-virus vaccines, which produce antigens in host cells, and (2) protein-based vaccines including inactivated whole virus and protein subunit vaccine, whose antigens are manufactured *in vitro* (Graham, 2020). Protein subunit vaccines have been traditionally used for vaccine development and such vaccines have good safety and effectiveness profiles in preventing diseases such as hepatitis B and herpes zoster (Syed, 2018; Valenzuela et al., 1982). Here, we reported the design of CoV RBD-sc-dimer as a protein subunit vaccine, representing a promising pathway for CoV vaccine development.

Structure-guided antigen design is an important tool to make vaccines with speed and precision (Graham, 2020). Full-length S protein is another common choice as CoV antigen subunit. Full-length trimeric S protein is usually highly immunogenic due likely to its large size (~600 kDa). It contains not only RBD, the major target for potent neutralizing antibodies, but also non-RBD regions that can also induce neutralizing or protective antibodies, for instance, the N-terminal domain (Chen et al., 2017; Pallesen et al., 2017; Wang et al., 2019; Zhou et al., 2019a). A generalized strategy was reported to stabilize pre-fusion conformation of MERS-CoV S protein via structure-based antigen design that improved the efficacy of full-length S protein-based CoV vaccine (Pallesen et al., 2017). However, because antibody-dependent enhancement (ADE) has been reported for CoV immune response (Corapi et al., 1992; Hohdatsu et al., 1998; Jaume et al., 2011; Kam et al., 2007; Vennema et al., 1990; Wan et al., 2020; Wang et al., 2014), minimized effective immunogens are sought. Alternatively, the RBD of CoV S protein has been recognized as an attractive vaccine target because of its advantages in immune focusing (Du et al., 2009a; Jiang et al., 2012; Ma et al., 2014; Wang et al., 2020b; Zhang et al., 2015; Zhou et al., 2019b),
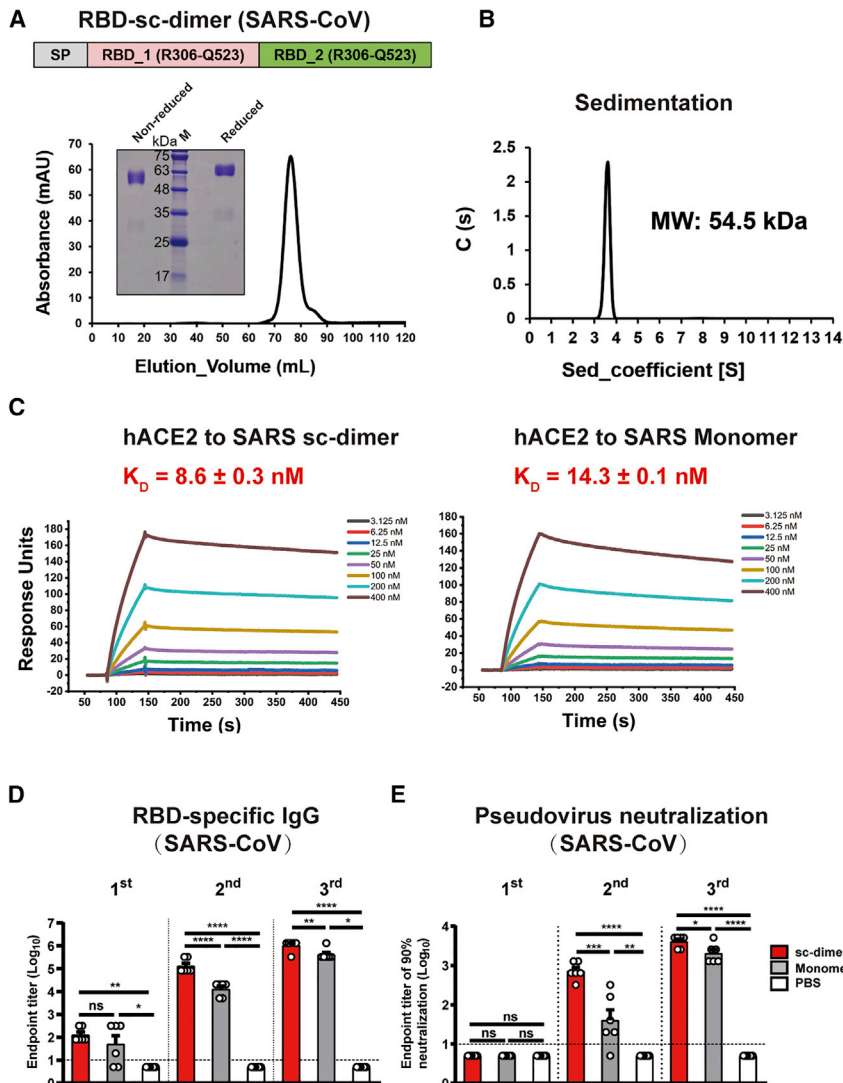
Figure 4. Design and Assessment of RBD-SC-Dimer as Vaccine against SARS-CoV

(A) A schematic diagram of SARS-CoV RBD-sc-dimer. Two SARS-CoV RBD (R306-Q523) were dimerized as tandem repeat (SP, signal peptide). Analytical gel filtration of SARS-CoV RBD-sc-dimer proteins was performed with HiLoad 16/600 Superdex 200 pg. The 280-nm absorbance curve is shown. Non-reduced and reduced SDS-PAGE migration profiles of the pooled samples are shown.

(B) Ultracentrifugation sedimentation profiles of SARS-CoV RBD-sc-dimer.

(C) Representative BIAcore diagrams of SARS-CoV RBD-sc-dimer and monomer bound to hACE2 protein. The K_D value was calculated by the software BIAevaluation Version 4.1 (GE Healthcare). The values shown are mean ± SD of two independent experiments.

(D and E) Groups of BALB/c mice were immunized with 10 μg dose of SARS-CoV RBD-sc-dimer and conventional RBD-monomer, respectively, with AddaVax as adjuvant. PBS formulated with adjuvant was given as control. A three-dose vaccination regimen was performed. Serum samples were collected after each immunization (19 days after 1st immunization, 14 days after 2nd immunization, and 14 days after 3rd immunization) to evaluate the humoral response dynamics. ELISA assay shows the SARS-CoV RBD specific IgG titers in (D) and SARS-CoV pseudovirus neutralization assay shows the NT_{90} in (E). The values shown in (D) and (E) are the mean ± SEM. The horizontal dashed line indicates the limit of detection. P-values were analyzed with one-way ANOVA (ns, $p > 0.05$; *$p < 0.05$; **$p < 0.01$; ***$p < 0.001$; ****$p < 0.0001$). See also Figure S2.

higher antibody response (**$p < 0.01$) and NAb titer (*$p < 0.05$) after three immunizations (Figures 4D and 4E).

The enhanced immunogenicity of RBD-sc-dimer could be explained by (1) doubling the molecular weight of antigen from ~30 kDa to ~60 kDa, (2) dual RBMs, by which the dimer works bivalently, that may cross-link B cell receptors in B cells for a better stimulation, (3) non-RBM epitopes on dimer-interface of RBD are likely occluded to further improve immune focusing, and (4) exposure of the immunodominant epitopes.

We provided a universal strategy to design beta-CoV vaccines and proved the concept in vaccine development against MERS, COVID-19, and SARS. The resulting immunogens could be applied to other expression systems such as yeast and insect cells and also to other vaccine platforms, like DNA, messenger RNA, and vaccine vectors. RBD-sc-dimer engineered without introduction of any exogenous sequence highlighted the feasibility for clinical development of RBD-sc-dimer-based CoV vaccines. The COVID-19 and MERS vaccine candidates described here are of promise for further development from bench to clinic. The antigen yields at g/L level highlight the scale-up production

but may require effective adjuvant and multiple doses to evoke adequate immunogenicity. We identified the disulfide-linked RBD-dimer as immunogen that significantly increased the immunogenicity compared to the conventional monomer as evidenced by NAb titers. The RBD-dimer was further engineered as a tandem repeat sc-dimer by a structure-guided design, which can be a generalizable strategy for beta-CoV vaccine design. Actually, two immunizations of RBD-sc-dimers were already sufficient to maximize high levels of antibody responses for all tested vaccines against MERS, COVID-19, and SARS (Figures 2F, 2G, 3D, 3E, 4D, and 4E). Thereby, a two-dose vaccination regimen will be applied to evaluate the protective efficacy in animal models and humans for the RBD-sc-dimer-based CoV vaccines. Of note, after three immunizations, the monomeric RBD is similar in terms of immunogenicity as two vaccinations with the sc-dimer. In particular, for SARS-CoV vaccine, RBD-sc-dimer showed only marginally

A

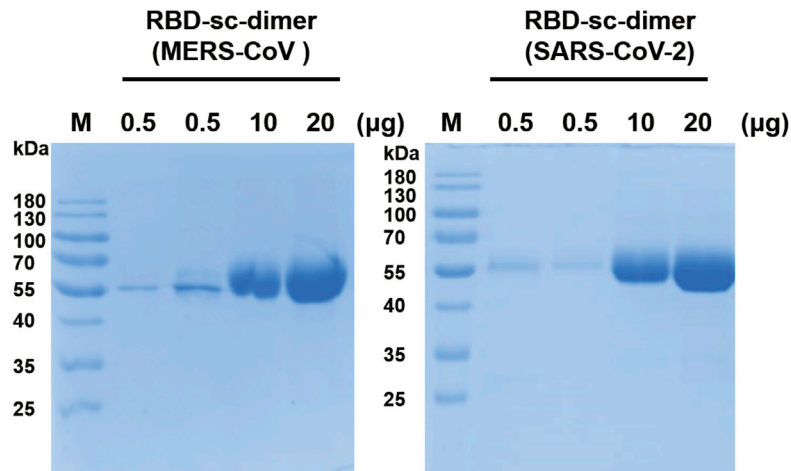|	Immunogen yields (g/L)	Purity
MERS-CoV	1.05	> 98%
SARS-CoV-2	0.67	> 98%

B

Figure 5. Pilot Scale Production of RBD-SC-Dimers of MERS-CoV and SARS-CoV-2
(A) RBD-sc-dimers were produced in industry-standard CHO cell system in GMP grade manufacturing. The immunogen yields and purities for vaccine stock solution are shown.
(B) Non-reduced SDS-PAGE migration profile of increasing amounts of GMP grade RBD-sc-dimers are shown.

capacity to meet the urgently global demands, in particular, for the pandemic COVID-19.

Limitations of Study

It is known that CoV RBD is the major target for NAbs interfering with viral receptor binding, and we were focusing on the humoral response induced by the RBD-based vaccines. An extended study (e.g., by passive transfer experiment) should be performed to further confirm whether the humoral response is sufficient to protect against CoV challenge, although our recent work by using human-origin monoclonal antibodies confirmed the passive protection (Shi et al., 2020; Wu et al., 2020). Although both PBS alone and PBS with adjuvant have been widely used as the placebo in studies of recombinant protein-based vaccines, groups receiving irrelevant protein with adjuvant are a better negative control.

STAR★METHODS

Detailed methods are provided in the online version of this paper and include the following:

- ● KEY RESOURCES TABLE
- ● RESOURCE AVAILABLITY
  - ○ Lead Contact
  - ○ Materials Availability
  - ○ Data and Code Availability
- ● EXPERIMENTAL MODEL AND SUBJECT DETAILS
  - ○ Cells and viruses
  - ○ Mice

- ● METHOD DETAILS
  - ○ Protein expression and purification
  - ○ Ethics statement
  - ○ Mouse experiments
  - ○ ELISA
  - ○ Pseudovirus neutralization assay
  - ○ Live SARS-CoV-2 and MERS-CoV neutralization assay
  - ○ Determination of virus titer in lung tissue samples
  - ○ Histopathology analysis
  - ○ ELISPOT
  - ○ ICS and flow cytometry
  - ○ Crystallization and structure determination
  - ○ SPR
  - ○ Analytical ultracentrifugation
  - ○ Pilot scale production of RBD-sc-dimers
  - ○ Sequences used in the alignments
- ● QUANTIFICATION AND STATISTICAL ANALYSIS

BL19U beamlines at National Center for Protein Sciences Shanghai and Shanghai Synchrotron Radiation Facility (Shanghai, China) for assistance during data collection. This work is supported by the National Natural Science Foundation of China, China (NSFC) (81991494), the National Science and Technology Major Project, China (2016YFE0205800 and 2018ZX10101-004), and the Strategic Priority Research Program of the CAS, China (XDPB0301). L. Dai is supported by Youth Innovation Promotion Association CAS, China (2018113).

AUTHOR CONTRIBUTIONS

DECLARATION OF INTERESTS

REFERENCES

Adams, P.D., Afonine, P.V., Bunkóczi, G., Chen, V.B., Davis, I.W., Echols, N., Headd, J.J., Hung, L.W., Kapral, G.J., Grosse-Kunstleve, R.W., et al. (2010). PHENIX: a comprehensive Python-based system for macromolecular structure solution. Acta Crystallogr. D Biol. Crystallogr. 66, 213–221.

Banerjee, A., Kulcsar, K., Misra, V., Frieman, M., and Mossman, K. (2019). Bats and Coronaviruses. Viruses 11, 41.

Chen, Y., Lu, S., Jia, H., Deng, Y., Zhou, J., Huang, B., Yu, Y., Lan, J., Wang, W., Lou, Y., et al. (2017). A novel neutralizing monoclonal antibody targeting the N-terminal domain of the MERS-CoV spike protein. Emerg. Microbes Infect. 6, e37.

Chiu, S.S., Chan, K.H., Chu, K.W., Kwan, S.W., Guan, Y., Poon, L.L., and Peiris, J.S. (2005). Human coronavirus NL63 infection and other coronavirus infections in children hospitalized with acute respiratory disease in Hong Kong, China. Clin. Infect. Dis. 40, 1721–1729.

Collaborative Computational Project, Number 4 (1994). The CCP4 suite: programs for protein crystallography. Acta Crystallogr. D Biol. Crystallogr. 50, 760–763.

Corapi, W.V., Olsen, C.W., and Scott, F.W. (1992). Monoclonal antibody analysis of neutralization and antibody-dependent enhancement of feline infectious peritonitis virus. J. Virol. 66, 6695–6705.

Du, L., Zhao, G., He, Y., Guo, Y., Zheng, B.J., Jiang, S., and Zhou, Y. (2007). Receptor-binding domain of SARS-CoV spike protein induces long-term protective immunity in an animal model. Vaccine 25, 2832–2838.

Du, L., He, Y., Zhou, Y., Liu, S., Zheng, B.J., and Jiang, S. (2009a). The spike protein of SARS-CoV–a target for vaccine and therapeutic development. Nat. Rev. Microbiol. 7, 226–236.

Du, L., Zhao, G., Chan, C.C., Sun, S., Chen, M., Liu, Z., Guo, H., He, Y., Zhou, Y., Zheng, B.J., and Jiang, S. (2009b). Recombinant receptor-binding domain of SARS-CoV spike protein expressed in mammalian, insect and E. coli cells elicits potent neutralizing antibody and protective immunity. Virology 393, 144–150.

Du, L., Kou, Z., Ma, C., Tao, X., Wang, L., Zhao, G., Chen, Y., Yu, F., Tseng, C.T., Zhou, Y., and Jiang, S. (2013). A truncated receptor-binding domain of MERS-CoV spike protein potently inhibits MERS-CoV infection and induces strong neutralizing antibody responses: implication for developing therapeutics and vaccines. PLoS ONE 8, e81587.

Emsley, P., and Cowtan, K. (2004). Coot: model-building tools for molecular graphics. Acta Crystallogr. D Biol. Crystallogr. 60, 2126–2132.

Gorse, G.J., O'Connor, T.Z., Hall, S.L., Vitale, J.N., and Nichol, K.L. (2009). Human coronavirus and acute respiratory illness in older adults with chronic obstructive pulmonary disease. J. Infect. Dis. 199, 847–857.

Graham, B.S. (2020). Rapid COVID-19 vaccine development. Science 368, 945–946.

He, Y., Zhou, Y., Liu, S., Kou, Z., Li, W., Farzan, M., and Jiang, S. (2004). Receptor-binding domain of SARS-CoV spike protein induces highly potent neutralizing antibodies: implication for developing subunit vaccine. Biochem. Biophys. Res. Commun. 324, 773–781.

Hoffmann, M., Kleine-Weber, H., Schroeder, S., Kruger, N., Herrler, T., Erichsen, S., Schiergens, T.S., Herrler, G., Wu, N.H., Nitsche, A., et al. (2020). SARS-CoV-2 cell entry depends on ACE2 and TMPRSS2 and is blocked by a clinically proven protease inhibitor. Cell 181, 271–280.

Hohdatsu, T., Yamada, M., Tominaga, R., Makino, K., Kida, K., and Koyama, H. (1998). Antibody-dependent enhancement of feline infectious peritonitis virus infection in feline alveolar macrophages and human monocyte cell line U937 by serum of cats experimentally or naturally infected with feline coronavirus. J. Vet. Med. Sci. 60, 49–55.

Hwang, W.C., Lin, Y., Santelli, E., Sui, J., Jaroszewski, L., Stec, B., Farzan, M., Marasco, W.A., and Liddington, R.C. (2006). Structural basis of neutralization by a human anti-severe acute respiratory syndrome spike protein antibody, 80R. J. Biol. Chem. 281, 34610–34616.

Jaume, M., Yip, M.S., Cheung, C.Y., Leung, H.L., Li, P.H., Kien, F., Dutry, I., Callendret, B., Escriou, N., Altmeyer, R., et al. (2011). Anti-severe acute respiratory syndrome coronavirus spike antibodies trigger infection of human immune cells via a pH- and cysteine protease-independent FcγR pathway. J. Virol. 85, 10582–10597.

Jean, A., Quach, C., Yung, A., and Semret, M. (2013). Severity and outcome associated with human coronavirus OC43 infections among children. Pediatr. Infect. Dis. J. 32, 325–329.

Jevšnik, M., Uršič, T., Zigon, N., Lusa, L., Krivec, U., and Petrovec, M. (2012). Coronavirus infections in hospitalized pediatric patients with acute respiratory tract disease. BMC Infect. Dis. 12, 365.

Jiang, S., Bottazzi, M.E., Du, L., Lustigman, S., Tseng, C.T., Curti, E., Jones, K., Zhan, B., and Hotez, P.J. (2012). Roadmap to developing a recombinant coronavirus S protein receptor-binding domain vaccine for severe acute respiratory syndrome. Expert Rev. Vaccines 11, 1405–1413.

Jiang, S., Hillyer, C., and Du, L. (2020). Neutralizing antibodies against SARS-CoV-2 and other human coronaviruses. Trends Immunol. 41, 355–359.

Kam, Y.W., Kien, F., Roberts, A., Cheung, Y.C., Lamirande, E.W., Vogel, L., Chu, S.L., Tse, J., Guarner, J., Zaki, S.R., et al. (2007). Antibodies against trimeric S glycoprotein protect hamsters against SARS-CoV challenge despite their capacity to mediate FcgammaRII-dependent entry into B cells in vitro. Vaccine 25, 729–740.

Kim, Y.S., Son, A., Kim, J., Kwon, S.B., Kim, M.H., Kim, P., Kim, J., Byun, Y.H., Sung, J., Lee, J., et al. (2018). Chaperna-mediated assembly of ferritin-based Middle East respiratory syndrome-coronavirus nanoparticles. Front. Immunol. 9, 1093.

Knipe, D.M., and Howley, P.M. (2013). Coronaviridae. Fields Virology, Sixth Edition (Lippincott Williams & Wilkins).

Lan, J., Ge, J., Yu, J., Shan, S., Zhou, H., Fan, S., Zhang, Q., Shi, X., Wang, Q., Zhang, L., and Wang, X. (2020). Structure of the SARS-CoV-2 spike receptor-binding domain bound to the ACE2 receptor. Nature 581, 215–220.

Li, W., Moore, M.J., Vasilieva, N., Sui, J., Wong, S.K., Berne, M.A., Somasundaran, M., Sullivan, J.L., Luzuriaga, K., Greenough, T.C., et al. (2003). Angiotensin-converting enzyme 2 is a functional receptor for the SARS coronavirus. Nature 426, 450–454.

Li, F., Li, W., Farzan, M., and Harrison, S.C. (2005a). Structure of SARS coronavirus spike receptor-binding domain complexed with receptor. Science 309, 1864–1868.

Li, M., Gao, F., Mascola, J.R., Stamatatos, L., Polonis, V.R., Koutsoukos, M., Voss, G., Goepfert, P., Gilbert, P., Greene, K.M., et al. (2005b). Human immunodeficiency virus type 1 env clones from acute and early subtype B infections for standardized assessments of vaccine-elicited neutralizing antibodies. J. Virol. 79, 10108–10125.

Li, Y., Wan, Y., Liu, P., Zhao, J., Lu, G., Qi, J., Wang, Q., Lu, X., Wu, Y., Liu, W., et al. (2015). A humanized neutralizing antibody against MERS-CoV targeting the receptor-binding domain of the spike protein. Cell Res. 25, 1237–1249.

Li, E., Chi, H., Huang, P., Yan, F., Zhang, Y., Liu, C., Wang, Z., Li, G., Zhang, S., Mo, R., et al. (2019). A novel bacterium-like particle vaccine displaying the MERS-CoV receptor-binding domain induces specific mucosal and systemic immune responses in mice. Viruses 11, 799.

Lu, G., Hu, Y., Wang, Q., Qi, J., Gao, F., Li, Y., Zhang, Y., Zhang, W., Yuan, Y., Bao, J., et al. (2013). Molecular basis of binding between novel human coronavirus MERS-CoV and its receptor CD26. Nature 500, 227–231.

Lu, G., Wang, Q., and Gao, G.F. (2015). Bat-to-human: spike features determining 'host jump' of coronaviruses SARS-CoV, MERS-CoV, and beyond. Trends Microbiol. 23, 468–478.

Ma, C., Wang, L., Tao, X., Zhang, N., Yang, Y., Tseng, C.K., Li, F., Zhou, Y., Jiang, S., and Du, L. (2014). Searching for an ideal vaccine candidate among different MERS coronavirus receptor-binding fragments–the importance of immunofocusing in subunit vaccine design. Vaccine 32, 6170–6176.

Modjarrad, K., Moorthy, V.S., Ben Embarek, P., Van Kerkhove, M., Kim, J., and Kieny, M.P. (2016). A roadmap for MERS-CoV research and product development: report from a World Health Organization consultation. Nat. Med. 22, 701–705.

Nie, J., Li, Q., Wu, J., Zhao, C., Hao, H., Liu, H., Zhang, L., Nie, L., Qin, H., Wang, M., et al. (2020). Establishment and validation of a pseudovirus neutralization assay for SARS-CoV-2. Emerg. Microbes Infect. 9, 680–686.

Nyon, M.P., Du, L., Tseng, C.K., Seid, C.A., Pollet, J., Naceanceno, K.S., Agrawal, A., Algaissi, A., Peng, B.H., Tai, W., et al. (2018). Engineering a stable CHO cell line for the expression of a MERS-coronavirus vaccine antigen. Vaccine 36, 1853–1862.

Otwinowski, Z., and Minor, W. (1997). Processing of X-ray diffraction data collected in oscillation mode. Methods Enzymol. 276, 307–326.

Pallesen, J., Wang, N., Corbett, K.S., Wrapp, D., Kirchdoerfer, R.N., Turner, H.L., Cottrell, C.A., Becker, M.M., Wang, L., Shi, W., et al. (2017). Immunogenicity and structures of a rationally designed prefusion MERS-CoV spike antigen. Proc. Natl. Acad. Sci. USA 114, E7348–E7357.

Raj, V.S., Mou, H., Smits, S.L., Dekkers, D.H., Müller, M.A., Dijkman, R., Muth, D., Demmers, J.A., Zaki, A., Fouchier, R.A., et al. (2013). Dipeptidyl peptidase 4 is a functional receptor for the emerging human coronavirus-EMC. Nature 495, 251–254.

Read, R.J. (2001). Pushing the boundaries of molecular replacement with maximum likelihood. Acta Crystallogr. D Biol. Crystallogr. 57, 1373–1382.

Reed, L.J., and Muench, H. (1938). A simple method of estimating fifty percent endpoints. Am. J. Epidemiol. 27, 493–497.

Robert, X., and Gouet, P. (2014). Deciphering key features in protein structures with the new ENDscript server. Nucleic Acids Res. 42, W320-4.

Shang, J., Ye, G., Shi, K., Wan, Y., Luo, C., Aihara, H., Geng, Q., Auerbach, A., and Li, F. (2020). Structural basis of receptor recognition by SARS-CoV-2. Nature 581, 221–224.

Shi, R., Shan, C., Duan, X., Chen, Z., Liu, P., Song, J., Song, T., Bi, X., Han, C., Wu, L., et al. (2020). A human neutralizing antibody targets the receptor binding site of SARS-CoV-2. Nature. Published online May 26, 2020. https://doi.org/10.1038/s41586-020-2381-y.

Syed, Y.Y. (2018). Recombinant zoster vaccine (Shingrix®): A review in herpes zoster. Drugs Aging 35, 1031–1040.

Tai, W., Zhao, G., Sun, S., Guo, Y., Wang, Y., Tao, X., Tseng, C.K., Li, F., Jiang, S., Du, L., and Zhou, Y. (2016). A recombinant receptor-binding domain of MERS-CoV in trimeric form protects human dipeptidyl peptidase 4 (hDPP4) transgenic mice from MERS-CoV infection. Virology 499, 375–382.

Tang, J., Zhang, N., Tao, X., Zhao, G., Guo, Y., Tseng, C.T., Jiang, S., Du, L., and Zhou, Y. (2015). Optimization of antigen dose for a receptor-binding domain-based subunit vaccine against MERS coronavirus. Hum. Vaccin. Immunother. 11, 1244–1250.

Valenzuela, P., Medina, A., Rutter, W.J., Ammerer, G., and Hall, B.D. (1982). Synthesis and assembly of hepatitis B virus surface antigen particles in yeast. Nature 298, 347–350.

Vennema, H., de Groot, R.J., Harbour, D.A., Dalderup, M., Gruffydd-Jones, T., Horzinek, M.C., and Spaan, W.J. (1990). Early death after feline infectious peritonitis virus challenge due to recombinant vaccinia virus immunization. J. Virol. 64, 1407–1409.

Walls, A.C., Park, Y.J., Tortorici, M.A., Wall, A., McGuire, A.T., and Veesler, D. (2020). Structure, function, and antigenicity of the SARS-CoV-2 spike glycoprotein. Cell 181, 281–292.

Wan, Y., Shang, J., Sun, S., Tai, W., Chen, J., Geng, Q., He, L., Chen, Y., Wu, J., Shi, Z., et al. (2020). Molecular mechanism for antibody-dependent enhancement of coronavirus entry. J. Virol. 94, e02015–e02019.

Wang, N., Shi, X., Jiang, L., Zhang, S., Wang, D., Tong, P., Guo, D., Fu, L., Cui, Y., Liu, X., et al. (2013). Structure of MERS-CoV spike receptor-binding domain complexed with human receptor DPP4. Cell Res. 23, 986–993.

Wang, S.F., Tseng, S.P., Yen, C.H., Yang, J.Y., Tsao, C.H., Shen, C.W., Chen, K.H., Liu, F.T., Liu, W.T., Chen, Y.M., and Huang, J.C. (2014). Antibody-dependent SARS coronavirus infection is mediated by antibodies against spike proteins. Biochem. Biophys. Res. Commun. 451, 208–214.

Wang, C., Zheng, X., Gai, W., Wong, G., Wang, H., Jin, H., Feng, N., Zhao, Y., Zhang, W., Li, N., et al. (2017). Novel chimeric virus-like particles vaccine displaying MERS-CoV receptor-binding domain induce specific humoral and cellular immune response in mice. Antiviral Res. 140, 55–61.

Wang, N., Rosen, O., Wang, L., Turner, H.L., Stevens, L.J., Corbett, K.S., Bowman, C.A., Pallesen, J., Shi, W., Zhang, Y., et al. (2019). Structural definition of a neutralization-sensitive epitope on the MERS-CoV S1-NTD. Cell Rep. 28, 3395–3405.

Wang, C., Horby, P.W., Hayden, F.G., and Gao, G.F. (2020a). A novel coronavirus outbreak of global health concern. Lancet 395, 470–473.

Wang, N., Shang, J., Jiang, S., and Du, L. (2020b). Subunit vaccines against emerging pathogenic human coronaviruses. Front. Microbiol. 11, 298.

Wang, Q., Zhang, Y., Wu, L., Niu, S., Song, C., Zhang, Z., Lu, G., Qiao, C., Hu, Y., Yuen, K.Y., et al. (2020c). Structural and functional basis of SARS-CoV-2 entry by using human ACE2. Cell 181, 894–904.

Wei, Q., Wang, Y., Ma, J., Han, J., Jiang, M., Zhao, L., Ye, F., Song, J., Liu, B., Wu, L., et al. (2020). Description of the first strain of 2019-nCoV, C-Tan-nCoV Wuhan strain-National Pathogen Resource Center, China, 2020. China CDC Weekly 2, 61–62.

Wevers, B.A., and van der Hoek, L. (2009). Recently discovered human coronaviruses. Clin. Lab. Med. 29, 715–724.

Williams, C.J., Headd, J.J., Moriarty, N.W., Prisant, M.G., Videau, L.L., Deis, L.N., Verma, V., Keedy, D.A., Hintze, B.J., Chen, V.B., et al. (2018). MolProbity: More and better reference data for improved all-atom structure validation. Protein Sci. 27, 293–315.

Wong, A.C.P., Li, X., Lau, S.K.P., and Woo, P.C.Y. (2019). Global epidemiology of bat coronaviruses. Viruses 11, 174.

Woo, P.C., Lau, S.K., Lam, C.S., Lai, K.K., Huang, Y., Lee, P., Luk, G.S., Dyrting, K.C., Chan, K.H., and Yuen, K.Y. (2009). Comparative analysis of complete genome sequences of three avian coronaviruses reveals a novel group 3c coronavirus. J. Virol. 83, 908–917.

Wu, Y., Wang, F., Shen, C., Peng, W., Li, D., Zhao, C., Li, Z., Li, S., Bi, Y., Yang, Y., et al. (2020). A noncompeting pair of human neutralizing antibodies block COVID-19 virus binding to its receptor ACE2. Science *368*, 1274–1278.

Xiao, X., Feng, Y., Chakraborti, S., and Dimitrov, D.S. (2004). Oligomerization of the SARS-CoV S glycoprotein: dimerization of the N-terminus and trimerization of the ectodomain. Biochem. Biophys. Res. Commun. *322*, 93–99.

Yan, R., Zhang, Y., Li, Y., Xia, L., Guo, Y., and Zhou, Q. (2020). Structural basis for the recognition of SARS-CoV-2 by full-length human ACE2. Science *367*, 1444–1448.

Yuan, Y., Cao, D., Zhang, Y., Ma, J., Qi, J., Wang, Q., Lu, G., Wu, Y., Yan, J., Shi, Y., et al. (2017). Cryo-EM structures of MERS-CoV and SARS-CoV spike glycoproteins reveal the dynamic receptor binding domains. Nat. Commun. *8*, 15092.

Zhang, N., Tang, J., Lu, L., Jiang, S., and Du, L. (2015). Receptor-binding domain-based subunit vaccines against MERS-CoV. Virus Res. *202*, 151–159.

Zhang, S., Zhou, P., Wang, P., Li, Y., Jiang, L., Jia, W., Wang, H., Fan, A., Wang, D., Shi, X., et al. (2018). Structural definition of a unique neutralization epitope on the receptor-binding domain of MERS-CoV spike glycoprotein. Cell Rep. *24*, 441–452.

Zhao, J., Li, K., Wohlford-Lenane, C., Agnihothram, S.S., Fett, C., Zhao, J., Gale, M.J., Jr., Baric, R.S., Enjuanes, L., Gallagher, T., et al. (2014). Rapid generation of a mouse model for Middle East respiratory syndrome. Proc. Natl. Acad. Sci. USA *111*, 4970–4975.

Zhou, H., Chen, Y., Zhang, S., Niu, P., Qin, K., Jia, W., Huang, B., Zhang, S., Lan, J., Zhang, L., et al. (2019a). Structural definition of a neutralization epitope on the N-terminal domain of MERS-CoV spike glycoprotein. Nat. Commun. *10*, 3068.

Zhou, Y., Yang, Y., Huang, J., Jiang, S., and Du, L. (2019b). Advances in MERS-CoV vaccines and therapeutics based on the receptor-binding domain. Viruses *11*, E60.

Zhu, N., Zhang, D., Wang, W., Li, X., Yang, B., Song, J., Zhao, X., Huang, B., Shi, W., Lu, R., et al.; China Novel Coronavirus Investigating and Research Team (2020). A novel coronavirus from patients with pneumonia in China, 2019. N. Engl. J. Med. *382*, 727–733.

STAR★METHODS

KEY RESOURCES TABLE

REAGENT or RESOURCE	SOURCE	IDENTIFIER
Antibodies		
Goat pAb to Ms IgG (HRP)	Abcam	Cat#ab6789; RRID: AB_955439
Mouse IFN-γ ELISPOT Pair	BD Biosciences	Cat#551881
APC-Cy7 Rat Anti-Mouse CD4	BD Biosciences	Cat#552051; RRID: AB_394331
APC Rat Anti-Mouse IL-2	BD Biosciences	Cat#554429; RRID: AB_398555
PE Rat Anti-Mouse IFN-γ	BD Biosciences	Cat#554412; RRID: AB_395376
PE/Cyanine7 anti-mouse TNF-α Antibody	BioLegend	Cat#506324; RRID: AB_2256076
FITC anti-mouse CD3 Antibody	BioLegend	Cat#100204; RRID: AB_312661
PerCP/Cyanine5.5 anti-mouse CD8a Antibody	BioLegend	Cat#100734; RRID: AB_2075238
PE anti-mouse IL-4 Antibody	BioLegend	Cat#504104; RRID: AB_315318
Bacterial and Virus Strains		
MERS-CoV hCoV-EMC2012 strain	Provided by Professor Ron Fouchier, Erasmus Medical Centre, Rotterdam, Netherlands	N/A
SARS-CoV-2 2020XN4276 strain	Isolated from throat swab of a SARS-CoV-2 infected patient by Guangdong CDC, China	N/A
MERS-CoV pseudovirus	This paper	N/A
SARS-CoV-2 pseudovirus	This paper	N/A
SARS-CoV pseudovirus	This paper	N/A
Ad5-hCD26	Provided by Dr.Tan Wenjie, China CDC	N/A
MAX Efficiency DH10Bac Competent *E.coli*	Invitrogen	Cat#10361-012
Biological Samples		
Serum samples from BALB/c mice	This paper	N/A
Lungs from BALB/c mice	This paper	N/A
Chemicals, Peptides, and Recombinant Proteins		
PEI	Alfa	Cat#A04043896-1g
AddaVax adjuvant	InvivoGen, USA	Cat#vac-adx-10
Imject Alum adjuvant	Thermo Scientific, USA	Cat#77161
Recombinant MERS-CoV-S protein RBD monomer (baculovirus-expressed), spike residues 367-606, accession number: JX869059	This paper	N/A
Recombinant MERS-CoV-S protein RBD dimer (baculovirus-expressed), spike residues 367-606, accession number: JX869059	This paper	N/A
Recombinant MERS-CoV-S protein RBD monomer (mammalian cell-expressed), spike residues 367-606, accession number: JX869059	This paper	N/A
Recombinant MERS-CoV-S protein RBD-sc-dimer (mammalian cell-expressed), spike residues 367-602, two copies in tandem, accession number: JX869059	This paper	N/A
Recombinant SARS-CoV-2-S protein RBD monomer (mammalian cell-expressed), spike residues 319-541, accession number: YP_009724390	This paper	N/A
Recombinant SARS-CoV-2-S protein RBD-sc-dimer (mammalian cell-expressed), spike residues 319-537, two copies in tandem, accession number: YP_009724390	This paper	N/A

(Continued on next page)

Continued

REAGENT or RESOURCE	SOURCE	IDENTIFIER
Recombinant SARS-CoV-S protein RBD monomer (mammalian cell-expressed), spike residues 306-527, accession number: NP_828851	This paper	N/A
Recombinant SARS-CoV-S protein RBD-sc-dimer (mammalian cell-expressed), spike residues 306-523, two copies in tandem, accession number: NP_828851	This paper	N/A
Recombinant hCD26 (baculovirus-expressed), spike residues 39-766, accession number: NP_001926	This paper	N/A
Recombinant hACE2 protein (baculovirus-expressed), residues 19-615, accession number: BAJ21180	This paper	N/A
Recombinant hACE2 protein (mammalian cell-expressed), residues 1-740	Sino Biological Inc.	Cat#10108-H08H
Critical Commercial Assays		
HisTrap HP 5 ml column	GE Healthcare	Cat#17524802
Hiload® 16/600 Superdex® 200 PG column	GE Healthcare	Cat#28989335
Luciferase Assay System	Promega	Cat#E4550
GloMax® Microplate Luminometer	Promega	N/A
BIAcore® 3000	GE Healthcare	N/A
Sensor Chip CM5	GE Healthcare	Cat#29-1496-04
HRP Streptavidin	BD Biosciences	Cat#557630
ELISPOT AEC Substrate Set	BD Biosciences	Cat#551951
Deposited Data		
Crystal structure of MERS-CoV S protein RBD-dimer	This paper	PDB code 7C02
Experimental Models: Cell Lines		
Sf9 Cells, SFM Adapted	Invitrogen	Cat#11496015
High Five cells	Invitrogen	Cat#B85502
Huh7 cells	Institute of Basic Medical Sciences CAMS	Cat# 3111C0001CCC000679; RRID: CVCL_0336
HEK293T cells	ATCC	Cat#CRL-3216; RRID: CVCL_0063
Vero cells	ATCC	Cat#CCL-81; RRID: CVCL_0059
CHOZN® CHO K1 host cell line	SAFC	Cat#CHOK1-1VL
Experimental Models: Organisms/Strains		
BALB/c mice	Beijing Vital River Laboratory Animal Technology Co., Ltd. (licensed by Charles River)	N/A
Recombinant DNA		
pFastbac1	Invitrogen	Cat#10360014
pFastbac1-MERS-CoV-RBD-His, residues 367-606, accession number: JX869059	This paper	N/A
pFastbac1-hACE2-his, residues 19-615, accession number: BAJ21180	This paper	N/A
pFastbac1-hCD26-his, residues 39-766, accession number: NP_001926	This paper	N/A
pCAGGS	MiaoLingPlasmid	Cat#P0165
pCAGGS-MERS-CoV-RBD-His, residues 367-606, accession number: JX869059	This paper	N/A
pCAGGS-MERS-RBD-sc-dimer-His, residues 367-602, two copies in tandem, accession number: JX869059	This paper	N/A
pCAGGS-SARS-CoV-2-RBD-His, residues 319-541, accession number: YP_009724390	This paper	N/A

Continued

REAGENT or RESOURCE	SOURCE	IDENTIFIER
pCAGGS-SARS-CoV-2-RBD-sc-dimer-His, residues 319-537, two copies in tandem, accession number: YP_009724390	This paper	N/A
pCAGGS-SARS-CoV-RBD-His, residues 306-527, accession number: NP_828851	This paper	N/A
pCAGGS-SARS-RBD-sc-dimer-His, residues 306-523, two copies in tandem, accession number: NP_828851	This paper	N/A
pCAGGS-MERS-CoV-S, accession number: JX869059	This paper	N/A
pCAGGS-SARS-CoV-2-S, accession number: YP_009724390	This paper	N/A
pCAGGS-SARS-CoV-S, accession number: NP_828851	This paper	N/A
Software and Algorithms		
PyMOL software	The PyMOL Molecular Graphics System, Version 2.0 Schrödinger, LLC.	https://pymol.org/2/
BIAevaluation Version 4.1	GE Healthcare	N/A
ESPript 3	Robert and Gouet, 2014	http://espript.ibcp.fr/ESPript/ESPript/
GraphPad Prism 8.0	GraphPad Software	https://www.graphpad.com/
HKL2000	Otwinowski and Minor, 1997	N/A
Phaser	Read, 2001	N/A
Coot	Emsley and Cowtan, 2004	http://www2.mrclmb.cam.ac.uk/personal/peemsley/coot/
CCP4	Collaborative Computational Project, Number 4, 1994	http://www.ccp4.ac.uk/
Phenix	Adams et al., 2010	http://www.phenix-online.org/
MolProbity	Williams et al., 2018	N/A
OriginPro 2018	OriginLab Corporation	https://www.OriginLab.com

RESOURCE AVAILABLITY

Lead Contact
Further information and requests for resources and reagents should be directed to and will be fulfilled by the Lead Contact, George F. Gao (gaof@im.ac.cn).

Materials Availability
All requests for unique/stable reagents generated in this study should be directed to and will be fulfilled by the Lead Contact author with a completed Materials Transfer Agreement.

Data and Code Availability
The accession number for the atomic coordinates and diffraction data reported in this study is PDB code 7C02. All the other data supporting the finding of this study are available within the paper and are available from the corresponding author upon request.

EXPERIMENTAL MODEL AND SUBJECT DETAILS

Cells and viruses
African green monkey kidney epithelial cells (Vero cells) (ATCC), human embryonic kidney cells 293T (HEK293T cells) (ATCC) and Huh7 hepatoma cells (Institute of Basic Medical Sciences, CAMS) were maintained in Dulbecco's modified Eagle's medium (DMEM, Invitrogen, USA) supplemented with 10% fetal bovine serum (FBS) at 37°C under 5% CO_2. Sf9 (Invitrogen) and High five (Invitrogen) insect cells were cultured in Insect-XPRESS medium (Lonza, USA) at 28°C. CHOZN® CHO K1 cell line was purchased from Sigma-Aldrich(Shanghai)Trading Co., Ltd. CHOZN® CHO K1 cell line was authenticated and the other cell lines were not. All cell lines were tested negative for mycoplasma contamination. MERS-CoV (EMC2012 strain) and SARS-CoV-2 (2020XN4276 strain) were propagated in Vero cells.

Mice

Specific pathogen-free (SPF) 6-8-week old female BALB/c mice were purchased from Beijing Vital River Laboratory Animal Technology Co., Ltd. (licensed by Charles River). All mice used in this study are in good health and are not involved in other experimental procedure. They were housed under SPF conditions in the laboratory animal facilities at Institute of Microbiology, Chinese Academy of Science (IMCAS) and Institute of Laboratory Animal Sciences, Peking Union Medical College. Mice were housed with 6 companions per cage. All animals were allowed free access to water and standard chow diet and provided with a 12-hour light and dark cycle (temperature: 20-25°C, humidity: 40%–70%).

METHOD DETAILS

Protein expression and purification

The baculovirus expressed recombinant MERS-CoV RBD dimer, monomer proteins, hACE2 and hCD26 protein were expressed with the Bac-to-Bac baculovirus expression system (Invitrogen). The coding sequence for MERS-CoV RBD (S protein residues 367–606, GenBank: JX869059), hACE2 (residues 19−615, GenBank: BAJ21180) and hCD26 (residues 39-766, GenBank: NP_001926) were codon-optimized and cloned into the baculovirus transfer vector pFastBac1 (Invitrogen). For each construct, gp67 signal peptide sequence was added to the protein N terminus for protein secretion, and a hexa-His tag was added to the C terminus to facilitate further purification processes (Lu et al., 2013; Wang et al., 2020c).

Transfection and virus amplification were conducted with Sf9 cells, and the recombinant proteins were produced in High Five cells (Invitrogen) for 2 days. The cell supernatants were then collected and soluble proteins were recovered through a 5 mL HisTrap™ HP column (GE Healthcare). After removal of most of the impurities, the recovered proteins were further purified by gel-filtration chromatography using a HiLoad® 16/600 Superdex® 200 pg column (GE Healthcare) with a running buffer of 20mM Tris-HCl and 150 mM NaCl (pH 8.0).

The mammalian cell-expressed recombinant proteins were transiently expressed in HEK293T cells. The coding sequence for MERS-CoV RBD (S protein 367–606, GenBank: JX869059), SARS-CoV-2 RBD (S protein 319-541, GenBank: YP_009724390), SARS-CoV RBD (S protein 306-527, GenBank: NP_828851) were codon-optimized for mammalian cell expression and synthesized. RBD-sc-dimer of MERS-CoV was two RBD (S protein 367–602) connected as tandem repeat. RBD-sc-dimer of SARS-CoV-2 was two RBD (S protein residues 319–537) connected as tandem repeat. RBD-sc-dimer of SARS-CoV was two RBD (S protein residues 306–523) connected as tandem repeat. For each construct, signal peptide sequence of MERS-CoV S protein (S protein residues 1-17) was added to the protein N terminus for protein secretion, and a hexa-His tag was added to the C terminus to facilitate further purification processes. These constructs were synthesized by GENEWIZ, China. These constructs were cloned into the pCAGGS vector, respectively, and transiently transfected into HEK293T cells. After 3 days, the supernatant was collected and soluble protein was purified by Ni affinity chromatography using a HisTrap™ HP 5 mL column (GE Healthcare). The sample was further purified via gel filtration chromatography with HiLoad® 16/600 Superdex® 200 pg (GE Healthcare) in a buffer composed of 20 mM Tris-HCl (pH 8.0) and 150 mM NaCl. The eluted peaks were analyzed by SDS-PAGE for protein size and purity.

The hACE2 protein (residues 1-740, Genbank: NP_068576) is expressed from HEK293T cells with poly-histidine tag at the C terminus (Sino Biological Inc., China).

Ethics statement

Animal studies were approved by the Committee on the Ethics of Animal Experiments of the IMCAS, and conducted in compliance with the recommendations in the Guide for the Care and Use of Laboratory Animals of the IMCAS Ethics Committee. All challenge studies with MERS-CoV were approved by the Institutional Animal Care and Use Committee of the Institute of Laboratory Animal Science, Peking Union Medical College.

Mouse experiments

For immunization of mice, each antigen was diluted with PBS, mixed with an equal volume of Imject Alum adjuvant (Thermo Scientific, USA) or AddaVax adjuvant (InvivoGen, USA) and emulsified by a syringe. BALB/c mice were vaccinated via the intramuscular injection. Serum samples were collected after vaccination as indicated in figures legends.

For MERS-CoV challenge experiments, mice were lightly euthanized with isoflurane and intranasally transduced with 2.5×10^8 PFU of Ad5-hCD26 35 days after the last immunization for rapid generation of a mouse model of MERS-CoV infection (Zhao et al., 2014). Five days later, the transduced mice were infected with 5×10^5 PFU of MERS-CoV (EMC2012 strain) in a total volume of 50 μL of DMEM medium via the i.n. route. The mice were euthanized and necropsied 3 days after challenge. Lung tissues were harvested for virus titration (standard $TCID_{50}$ titration based on CPE) and pathological examination. All animal experiments with MERS-CoV challenge were conducted under animal biosafety level 3 (ABSL3) facility in Peking Union Medical College.

ELISA

ELISA plates (Corning, USA) were coated over-night with 3 μg/mL of SARS-CoV-2, MERS-CoV or SARS-CoV monomeric RBD protein in 0.05 M carbonate-bicarbonate buffer, pH 9.6, and blocked in 5% skim milk in PBS. Serum samples were diluted and added to each well. Plates were incubated with goat anti-mouse IgG-HRP antibody and developed with 3,3′,5,5′-tetramethylbenzidine

(TMB) substrate. Reactions were stopped with 2 M hydrochloric acid, and the absorbance was measured at 450 nm using a microplate reader (PerkinElmer, USA). The endpoint titer was defined as the highest reciprocal dilution of serum to give an absorbance greater than 2.5-fold of the background values. Antibody titer below the limit of detection was determined as half the limit of detection.

Pseudovirus neutralization assay

MERS-CoV, SARS-CoV-2 and SARS-CoV pseudovirus preparation and neutralization assay were carried out by a previously published method (Nie et al., 2020), with some modifications. Briefly, the plasmids of pNL4-3.luc.RE and pCAGGS-S (encoding for full-length S protein of MERS-CoV, SARS-CoV-2 or SARS-CoV) were co-transfected into 293T cells. After 48 hours, the supernatant containing pseudovirus was harvested, centrifuged and filtered through a 0.45 μM sterilized membrane. Single use aliquots were stored at -80°C. The $TCID_{50}$ was determined by infection of Huh7 cells (Li et al., 2005b). To evaluate the pseudovirus neutralization activity of mouse serum, heat-inactivated serum was 2-fold serially diluted and incubated with an equal volume of 100 $TCID_{50}$ pseudovirus at 37°C. The medium was also mixed with pseudovirus as control. Then the mixture was transferred to pre-plated Huh7 cell monolayers in 96-well plates. After incubation for 24 or 48 hours, the cells were lysed and luciferase activity was measured by the Luciferase Assay System (Promega, USA) according to the manufacturer's protocol. NT_{90} was defined as the highest reciprocal serum dilution at which the relative light units (RLUs) were reduced by greater than 90% compared with virus control wells. NT_{90} below the limit of detection was determined as half the limit of detection.

Live SARS-CoV-2 and MERS-CoV neutralization assay

The live virus neutralization assay was conducted in a BSL-3 facility. Briefly, sera from immunized mice was 2-fold (MERS-CoV neutralization assay) or 4-fold (SARS-CoV-2 neutralization assay) serially diluted and mixed with the same volume of MERS-CoV (100 $TCID_{50}$, EMC strain) or SARS-CoV-2 (100 $TCID_{50}$, 2020XN4276 strain), incubated at 37°C. Thereafter, 100 μL virus-serum mixture was transferred to pre-plated Vero cells in 96-well plates. Inoculated plates were incubated at 37°C for an additional 72 h, following which the CPE of the virus were observed microscopically at 40-fold magnification. The neutralization titers were defined as the reciprocal of serum dilution required for 50% neutralization of viral infection.

Determination of virus titer in lung tissue samples

Lung tissues were homogenized in 1 mL of DMEM medium and clarified by low-speed centrifugation at 4500 g for 30 minutes at 4°C. Virus titers were determined in Vero cells monolayers grown in 96-well plates. Vero cells were seeded (1.5×10^4/well) in a 96-well plate and incubated overnight at 37°C in a CO_2 incubator. Then, 100 μL of 10-fold serially diluted suspension was added to each well in quadruplicate. The virus was allowed to adsorb to the cells at 37°C for 1 hour. After adsorption, the viral inocula were removed, and 0.1 mL medium (DMEM, 2% FBS) was added to each well. The plates were incubated in a CO_2 incubator at 37°C for 3 days, after which the CPEs were observed microscopically at 40-fold magnification. The virus titer of each specimen, expressed as the $TCID_{50}$, was calculated by the Reed–Muench method (Reed and Muench, 1938).

Histopathology analysis

Three mice per group necropsies were performed according to a standard protocol three days post infection. Lungs from challenged mice were collected, fixed in 10% neutral buffered formaldehyde, and embedded in paraffin. Tissue sections (5 μm) were stained with hematoxylin and eosin (H&E) and analyzed microscopically at 100-fold magnification. Lung injury was evaluated for peribronchiolitis (inflammatory cells, primarily lymphocytes, surrounding a bronchiole), perivasculitis (inflammatory cells, primarily lymphocytes, surrounding a blood vessel), interstitial pneumonitis (increased thickness of alveolar walls associated with inflammatory cells, primarily neutrophils), and alveolitis (inflammatory cells, primarily neutrophils and macrophages, within alveolar spaces).

ELISPOT

To detect antigen-specific T lymphocyte responses, an IFN-γ-based ELISPOT assay was performed. Mice spleens were removed and splenocytes were isolated. Flat-bottom, 96-well plates were pre-coated with 10 μg/mL anti-mouse IFN-γ Ab (BD Biosciences, USA) overnight at 4°C and then blocked for 2 hours at 37°C. Mouse splenocytes were added to the plate (2×10^5/well). Then, different concentrations of peptide pool were added to the wells. Phytohemagglutinin (PHA) was added as a positive control. Cells incubated without stimulation were employed as a negative control. After 18 hours of incubation, the cells were removed, and the plates were processed in turn with biotinylated IFN-γ detection antibody (BD Biosciences, USA), streptavidin-HRP conjugate (BD Biosciences, USA), and AEC substrate (BD Biosciences, USA). When the colored spots were intense enough to be visually observed, the development was stopped by thoroughly rinsing samples with deionized water. The numbers of the spots were determined using an automatic ELISPOT reader and image analysis software (Cellular Technology Ltd.).

ICS and flow cytometry

Mouse splenocytes were added to the plated (1×10^6/well). A peptide pool consisting of 20-mers (overlapping by 10 amino acids) spanning the SARS-CoV-2-S RBD were synthesized. Mouse splenocytes were stimulated with the peptide pool for 2 hours. The cells were then incubated with GolgiStop (BD Biosciences, USA) for an additional 10 hours at 37°C. Then, the cells were harvested and

stained with anti-CD3 (BioLegend), anti-CD8α (BioLegend) and anti-CD4 (BD Biosciences) surface markers. The cells were subsequently fixed and permeabilized in permeabilizing buffer (BD Biosciences, USA). Half of the cells were stained with anti-IFN-γ (BD Biosciences), anti-IL-2 (BD Biosciences) and anti-TNF-α (BioLegend). Another half of the cells were stained with anti-IL-4 (Biolegend). All labeled lymphocytes were gated on a FACSAriaIII flow cytometer (BD Biosciences, USA).

Crystallization and structure determination

The baculovirus-expressed protein of MERS-CoV RBD-dimer was buffered in 20 mM Tris, 50 mM NaCl, pH 8.0. It was concentrated to 10 or 5 mg/mL for crystallization. Crystallization trials were performed in sitting drops of 600 nl. All crystals were obtained by mixing equal volumes of protein and reservoir solution, using a Mosquito LCP robot (TTP LabTech). Diffraction-quality crystals of MERS-CoV RBD-dimer were obtained at 18°C in condition consisting of 0.12 M ethylene glycols, 0.1 M imidazole and MES (acid), 30% v/v ethylene glycol plus PEG 8K at condition of pH 6.5 (Morpheus® MD1-46). All diffraction data were collected at the Shanghai Synchrotron Radiation Facility (BL19U beamlines) and processed with HKL2000 (Otwinowski and Minor, 1997).The structure was solved by the molecular replacement module of Phaser (Read, 2001) from the CCP4 program suite (Collaborative Computational Project, Number 4, 1994), with the previously reported structure of MERS-CoV RBD (PDB: 4KQZ) as the search models. Restrained rigid-body refinement with REFMAC5 (CCP4 suite) and manual model building with Coot (Emsley and Cowtan, 2004) were then performed. Further rounds of refinement were then done with Phenix. Refine (Adams et al., 2010). During model building and refinement, the program of MolProbity (Williams et al., 2018) was used to validate the stereochemistry of the structure. The data collection and structure refinement statistics are summarized in Table S1. The structural figures were generated using the PyMOL Molecular Graphics System, Version 2.0.

SPR

The SPR assys were carried out at 25°C using a BIAcore 3000 machine with CM5 chips (GE Healthcare). All proteins for SPR assays were exchanged to PBST buffer (10 mM Na2HPO4; 2 mM KH2PO4, pH 7.4; 137 mM NaCl; 2.7 mM KCl; 0.005% Tween 20). The RBD-monomer and RBD-sc-dimer of SARS-CoV-2, SARS-CoV and MERS-CoV were immobilized in pairs onto CM5 chips, respectively, at about 1000 response units (RUs). Gradient concentrations of hCD26 (from 3.125 to 200 nM for MERS-CoV RBD and RBD-sc-dimer) and hACE2 (from 0.78125nM to 200nM for SARS-CoV-2 RBD and RBD-sc-dimer, and from 3.125nM to 400 nM for SARS-CoV RBD and RBD-sc-dimer) were then used to flow over the chip surface at 30 μL/min and the real-time response was recorded. After each cycle, the sensor surface was regenerated using 7 μL of 10 mM NaOH. The binding kinetics were analyzed using 1:1 binding model with the software BIAevaluation Version 4.1 (GE Healthcare).

Analytical ultracentrifugation

Sedimentation velocity experiments were carried out on three samples (SARS-CoV-2 RBD-sc-dimer, MERS-CoV RBD-sc-dimer and SARS-CoV RBD-sc-dimer) using the ProteomeLab XL-I analytical ultracentrifuge (Beckman Coulter, Brea, CA). A volume of 380 μL of protein sample (A_{280} = 0.6 - 0.8) and 400 μL of matching buffer (20mM Tris, 150mM NaCl, pH8.0) were injected into appropriate channels of 12 mm double sector aluminum epoxy cells with sapphire windows. Solutions were centrifuged at 39,000 rpm at 20°C in an An-60Ti rotor for 8 hours. Scans were collected at 280 nm, with 3 minutes elapsed between each scan. Data were analyzed using the continuous sedimentation coefficient distribution c(s) model in SEDFIT software.

Pilot scale production of RBD-sc-dimers

The coding sequence for RBD-sc-dimer proteins of MERS-CoV and SARS-CoV-2 were codon-optimized for mammalian cell expression. For each construct, signal peptide sequence was added to the N terminus for protein secretion. Both constructs do not contain any tag sequence at C terminus. Clinical-grade CHO-K1 (SAFC) cell lines expressing RBD-sc-dimers of MERS-CoV and SARS-CoV-2 were generated and further selected for high expression clones by WISDOMAB Biopharmaceutical Co.Ltd, China. Cell lines with highest antigen expression were selected for large-scale immunogen production and purification by Anhui Zhifei Longcom Biopharmaceutical Co.Ltd, China.

Sequences used in the alignments

The accession numbers of the sequences used for analyzing the RBD sequences of beta-CoVs are as follows: MERS-CoV (GenBank: AFS88936), SARS-CoV (GenBank: AAS00003), SARS-CoV-2 (GenBank: QHR63290), Bat-CoV_HKU5 (GenBank: ABN10875), Rousettus_bat-CoV (GenBank: AOG30822), Bat-CoV_BM48-31 (GenBank: ADK66841), Bat-CoV_HKU9 (GenBank: ABN10911), Bat_Hp-betaCoV (GenBank: AIL94216), SARS-related-CoV (GenBank: APO40579), BtRs-Beta-CoV (GenBank: QDF43825), Bat-SARS-like-CoV (GenBank: ATO98231), SARS-like-CoV_WIV16 (GenBank: ALK02457), Bat-CoV (GenBank: ARI44804), BtR1-Beta-CoV (GenBank: QDF43815), HCoV_HKU1 (GenBank: AZS52618), MCoV_MHV1 (GenBank: ACN89742), BetaCoV_HKU24 (GenBank: AJA91217), HCoV_OC43 (GenBank: AAR01015), BetaCoV_Erinaceus (GenBank: AGX27810).

QUANTIFICATION AND STATISTICAL ANALYSIS

K_D values for SPR assays were calculated by the software BIAevaluation Version 4.1 (GE Healthcare), using 1:1 binding model. The values shown are mean ± SD of two independent experiments. Details can be found in figures legends.

Pseudovirus neutralization were conducted with at least duplicates. P-values were analyzed with one-way ANOVA with multiple comparisons for ELISA and pseudovirus neutralization, live virus neutralization and viral loads measurements. P-values were analyzed with unpaired t test for ELISPOT and ICS assays. Details can be found in figures legends.

Supplemental Figures
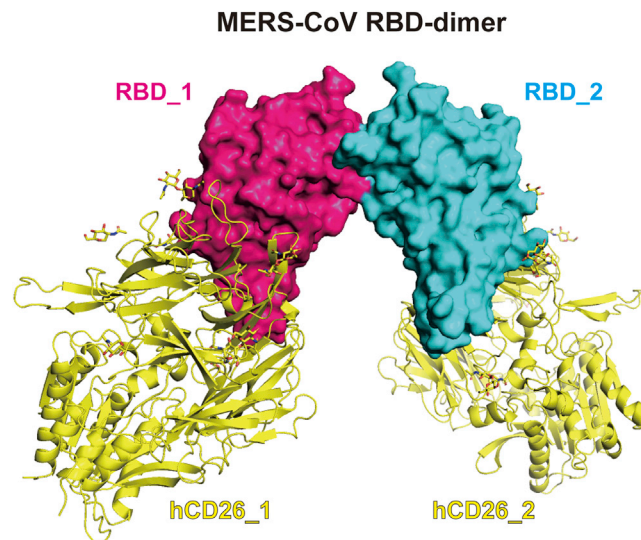
MERS-CoV RBD-dimer

Figure S1. MERS-CoV RBD-Dimer Fully Exposes Dual RBMs for Its Receptor hCD26, Related to Figure 2
The complex structure of hCD26/MERS-CoV-RBD (PDB: 4KR0) are docked onto MERS-CoV RBD dimer, showing the complete exposure of dual RBMs. Two RBD protomers are shown as surface and colored in hotpink and cyan, respectively. Two hCD26 are shown as cartoon and colored in yellow.
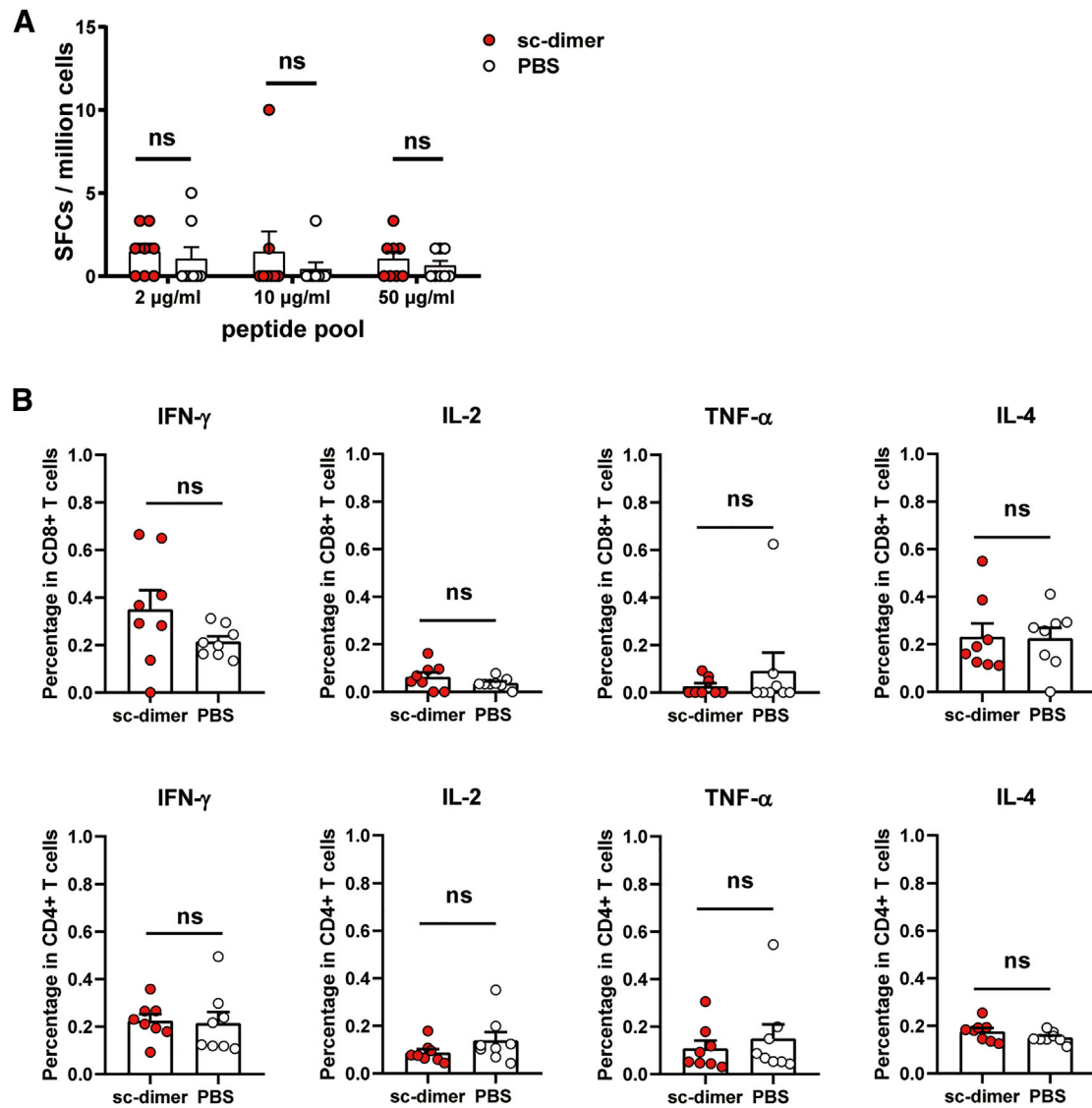
(legend on next page)

Figure S3. Characterization of the Cellular Immune Response for COVID-19 Vaccine, Related to Figure 3

Fourty-five after the last vaccination, the splenocytes were isolated from mice vaccinated with SARS-CoV-2 RBD-sc-dimer (plus AddaVax^TM adjuvant) and PBS (plus AddaVax^TM adjuvant), respectively.

(A) ELISPOT assay was performed to evaluate the ability of splenocytes to secrete IFN-γ following stimulation with different concentrations of peptide pool of SARS-CoV-2 RBD (2 μg/mL, 10 μg/mL and 50 μg/mL). Spot-forming cells (SFCs) per million cells are shown.

(B) An ICS assay was conducted to quantify the proportion of CD8+ and CD4+ T cells producing key cytokines (IFN-γ, IL-2, TNF-α and IL-4) following stimulation with 10 μg/mL peptide pool (SARS-CoV-2 RBD). Shown are the frequencies of respective cytokine-producing cells.

The values are the mean ± SEM. P-values were analyzed with unpaired t test (ns, p > 0.05).